Reports in Mechanical Engineering
Vol. 5, No. 1, 2024, pp. 43-67
ISSN: 2683-5894, DOI: https://doi.org/10.31181/rme324

Geometric Investigation of Thin Perforated Steel Plates Under Biaxial Elasto-Plastic Buckling by using Constructal Design

Thiago da Silveira[1], Cristiano Fragassa[2*], Luiz Alberto Oliveira Rocha[3,4], Elizaldo Domingues dos Santos[1], Liércio André Isoldi[1]

[1] School of Engineering, Universidade Federal do Rio Grande - FURG, Av Itália, km 8, s/n, 96203-900, Rio Grande, RS, Brazil.
[2] Department of Industrial Engineering, University of Bologna, Viale Risorgimento 2, 40136, Bologna, Italy.
[3] Department of Mechanical Engineering, Federal University of Rio Grande do Sul (UFRGS), Sarmento Leite St., 425, 90040-001, Porto Alegre-RS, Brazil.
[4] Institute of Earth Sciences, Complex Flow Systems Lab (CFS Lab), Rua Romao Ramalho 59, 7000-671 Evora, Portugal.

Article Info

Article history:

Received May 28, 2024
Revised July 19, 2024
Accepted August 19, 2024

Keywords:

Constructal Design
Elasto-plastic buckling
Biaxial plate buckling
Structural integrity
Thin-Walled Structures

ABSTRACT

In many structural engineering applications, perforated thin plates are commomly required, such as for cable and pipe passages or inspection windows, among other. It is well known that thin plates subjected to compressive loads may experience a structural instability called buckling, characterized by sudden out-of-plane displacements. To investigate this phenomenon and determine the optimal geometry of a thin steel plate featuring a centered elliptical opening, the Constructal Design (CD) method was applied in combination with the Exhaustive Search (ES) approach and the Finite Element Method (FEM). The CD method facilitates assessing geometric configurations to achieve the most effective distribution of imperfections, thereby maximizing the performance indicator relevant to this solid mechanics analysis. From the results of around 700 cases numerically simulated, it was observed that incorporating perforations impacts the mechanical strength of the plate by up to 62.5% when compared to an unperforated plate of identical dimensions (considered as a reference plate). In addition, plates without cutouts (reference plate), with different aspect ratios, the same thickness, the same amount of material, and the same normalized ultimate stress, can exhibit deflections with a difference of up to 229.4%.

Corresponding Author:

Cristiano Fragassa
Department of Industrial Engineering, University of Bologna, Viale Risorgimento 2, 40136, Bologna, Italy
Email: cristiano.fragassa@unibo.it

1. Introduction

Engineering structures are constantly evolving to provide better performances, maximizing variables like rigidity, strength, and stability, and minimizing costs and weight, among others. One of the most used components of structural engineering is the thin plate, with a wide application in civil, naval, aerospace, and automotive engineering. Thin plates are characterized by having in-plane dimensions much bigger than its thickness, t (Jones, 2006). In many practical applications, perforations in the plate are necessary (for purposes such as inspection, assembly, accommodating pipes, or reducing weight), which alters its mechanical behavior due to stress redistribution around the hole. (Shojaee et al., 2019). Tipically, these structures are subjected to compressive loads, which can cause the instability phenomenon known as buckling. According to Chajes and Åkesson, a thin plate does not collapse immediately after elastic buckling occurs, but it can sustain loads significantly higher than the critical load without experiencing excessive deformation (Åesson, 2014; Chajes, 1974). When it occurs, the load that defines the collapse of a plate, considering the elasto-plastic behavior, is called the ultimate or post-critical load and P_u represents it.

Since elasto-plastic buckling analysis of perforated plates is a complex task, the use of experimental or computational techniques is required. One of the most useful tools for this type of investigation is computational modeling via Finite Element Method (FEM), which can solve these problems with good accuracy and in various situations in a relatively short time compared to experimental methods. In addition, analytical solutions are mainly applied for very simple problems while experimental approach has the highest costs when compared to FEM. According to Liang and Yin the nonlinear finite element simulation is a standard technique for structural stability analysis, especially for large and complex structures (Liang & Yin, 2023). The significance and current relevance of this topic are underscored by numerous recent publications, including works by Qablan et al., Ghorbanhosseini et al., Guo and Yao, Musmar, Gore and Lokavarapu, Uslu et al., Zhang et al., Ipek et al., Saad-Eldeen and Garbatov, Shahani and Kiarasi, Cao et al., Figueiredo et al., Mishurenko and Semenov, Mitsui et al., and Wang et al. (Cao et al., 2024; Figueiredo, Simões, & da Costa, 2024; Ghorbanhosseini, Yaghoubi, & Bahrambeigi, 2021; Gore & Lokavarapu, 2022; Guo & Yao, 2021; Ipek et al., 2023; Mishurenko & Semenov, 2024; Mitsui, Ikarashi, & Sada, 2024; Musmar, 2021; Qablan et al., 2022; Saad-Eldeen & Garbatov, 2023; Shahani & Kiarasi, 2023; Uslu, Saraçoğlu, & Albayrak, 2022; Wang et al., 2024; Zhang et al., 2022). In this context, the present work seeks to optimize the geometries of centered elliptical perforations that provide the best mechanical behavior of simply-supported thin perforated steel plates when subjected to biaxial elasto-plastic buckling. For that, the FEM was used associated with the Constructal Design method (CD) and Exhaustive Search technique (ES). The CD is the method used to predict the evolutionary design and rhythm in any finite-size flow system, including nature, social, and engineering applications. It is used to demonstrate how the Constructal Law of design and evolution guides the design and its evolution over time (Rocha, Lorente, & Bejan, 2018).

The method uses constraints and degrees of freedom to define the search space for a geometric investigation, i.e., to define possible different geometric configurations for an engineering system, and performance indicators to identify how the design easily the internal currents (dos Santos et al., 2017). Therefore, all proposed geometries are analyzed regarding their performance through the comparison among the results numerically obtained by FEM, characterizing an optimization by ES technique. It is important to inform that the effectiveness of FEM, CD, and ES association to solve structural engineering problems was already proved by Da Silveira et al. (da Silveira et al., 2022). Given the above, the main original contribution of this work is the application of the CD method together with the ES technique and the FEM to understand the effects of the semi-axes ratio of the elliptical hole and the inclination angle of the cutout on the mechanical behavior of thin perforated steel plates with distinct aspect ratios and subjected to biaxial elasto-plastic buckling. To this end, a computational model was properly developed, verified, and validated to solve the complex phenomenon on biaxial elasto-plastic buckling of plates (with or without perforations), which is also a relevant scientific contribution to the state of the art. It is relevant to note that the adoption of the ES technique together with the CD method is a widely used approach because, in this way, it is possible not only to determine the optimal geometry, but also to evaluate and understand how the degrees of freedom influence the performance indicators. Several other potential optimization techniques allow obtaining the optimal geometry; however, this definition is reached without clearly understanding about the effect of the degrees of freedom variation on the performance indicators.

In addition, the ES technique was specifically chosen for this study due to its comprehensive nature, ensuring that “all” possible geometric configurations be explored to guarantee an optimal solution. While other optimization techniques, such as Genetic Algorithms or Particle Swarm Optimization, may offer faster results for large-scale problems, they can sometimes miss global optima or become overly dependent on initial conditions or parameter settings. In contrast, ES provides a complete evaluation of the solution space, which was crucial for our objective of obtaining precise and reliable results in the context of structural optimization. In summary, the following advantages of the ES technique can be highlighted: i) it ensures that the absolute best solution is identified by evaluating every possible configuration, unlike heuristic methods (e.g., Genetic Algorithms, Simulated Annealing), which may only find a near-optimal solution; ii) it is straightforward and easy to understand, making it accessible for researchers and practitioners without the need for deep knowledge of complex algorithms or parameter tuning; iii) it produces consistent results, as it does not rely on randomness or probabilistic processes, which can lead to varying outcomes in stochastic optimization techniques; iv) it does not require specific assumptions about the problem structure or solution landscape, making it applicable to a wide range of optimization problems without extensive customization; and v) it can be highly efficient for problems with a limited number of variables or configurations, providing a comprehensive analysis without the risk of missing critical solutions. However, if the goal is only to define the optimized geometry, without interest in understanding how this geometry was obtained, there is no need to use the ES (other optimization method can be employed). Therefore, the association of the CD with ES brings as main benefit the possibility of understand how the evolution of the geometric configuration, performed by the degrees of freedom variation, affect the performance indicators in such a way to obtain the best and the worst geometries.

2. Buckling and Post-Buckling Behavior of Plates

When subjected to compressive loads, slender mechanical structures can fail due to the buckling occurrence and, therefore, must be designed to avoid the failure caused by this undesirable instability phenomenon (Åesson, 2014; Chajes, 1974; Jones, 2006; Szilard, 2004). Although most structures, such as columns, have their failure determined by elastic buckling, for flat plates, a post-buckling behavior occurs for loads over the critical load of elastic buckling because it is a peculiar behavior of thin plates (Szilard, 2004; Trahair et al., 2017). Recent studies have explored various aspects of the buckling phenomenon in plates. Notable examples include Saad-Eldeen et al., who conducted experimental analyses on perforated plates with and without stiffeners under uniaxial buckling conditions, and Dong et al., who investigated local buckling in thin plates on tensionless elastic foundations subjected to combined uniaxial compression and shear (Dong et al., 2018; Saad-Eldeen, Garbatov, & Soares, 2018). Additionally, Milazzo et al. developed a single-domain model for the buckling and post-buckling behavior of cracked multilayered composite plates (Milazzo, Benedetti, & Gulizzi, 2018). Malikan and Nguyen and Farajpour et al. examined biaxial buckling in composite plates, while Kaveh et al., Moita et al., Ehsani and Dalir, and Kaveh et al. focused on optimizing the geometry of composite plates (Ehsani & Dalir, 2019; Farajpour, Shahidi, & Farajpour, 2018; Kaveh, Dadras, & Geran Malek, 2019; Kaveh, Dadras, & Malek, 2018; Malikan & Nguyen, 2018; Moita et al., 2018). Da Silva et al. analyzed hexagonally perforated thin steel plates under uniaxial elasto-plastic buckling, while Zureick and Hu et al. researched uniaxial buckling in thin steel plates (da Silva et al., 2019; Hu et al., 2020; Zureick, 2018). Lima et al. conducted a geometric analysis of thin steel plates with stiffeners under uniaxial elasto-plastic buckling (Lima et al., 2020). Yuan et al. introduced similarity criteria for predicting the entire buckling process of stiffened plates under compressive loads (Yuan et al., 2021). Furthermore, Falkowicz and Debski studied uniaxial buckling in composite plates, Hou et al. modeled the high-order buckling behavior of steel plate shear walls, and Zhang and Sun investigated the mechanical responses, including buckling, of a three-dimensional Maltese cross metamaterial (Falkowicz & Debski, 2021; Hou, Guo, & Yan, 2021; Zhang & Sun, 2023). Additional studies by Liang and Yin on nonlinear buckling in optimized wing structures, Jin et al. on the stability of composite plates bonded with graphene-reinforced actuators, and Park and Yi on a finite element analysis-based methodology for thin-plate buckling in crude oil tankers further contribute to the field. The wide range of applications of thin plates requires different engineering solutions (Jin, Leng, & Yang, 2024; Liang & Yin, 2023; Park & Yi, 2024). An example of this is the insertion of perforations to attend to many specific plate uses, like passage of pipes and cables, weight reduction, maintenance access, and assembling (Cheng & Zhao, 2010). Regarding the perforation's position, Mohammadzadeh et al. say that the critical load for uniaxial buckling is greater when the hole is positioned at the center of the plate compared to other locations (Mohammadzadeh, Choi, & Kim, 2018). Additionally, in post-buckling analyses of rectangular plates under biaxial compressive loads with a centrally placed cutout, the buckling resistance is found to be less than half of that under uniaxial loading. As noted by El-Sawy and Martini, this reduction is attributed to the redistribution of membrane stresses caused by the hole, which alters the buckling behavior of the plate (El-Sawy & Martini, 2010). It is worth mentioning that the complexity of the analysis and design of such structural components is high, especially when the perforation has an unusual shape and/or position, and it is even more complex if the problem conducts to an elasto-plastic buckling analysis. Nonetheless, computational modeling using the Finite Element Method (FEM) provides an accurate and effective approach to addressing these challenges (El-Sawy & Martini, 2010; Szilard, 2004). For example, Shanmugam et al. applied FEM to derive design equations for calculating the ultimate buckling load of square plates under axial and biaxial compression with centrally placed square and circular holes (Shanmugam & Narayanan, 1998). Their findings revealed that the ultimate load capacity of square perforated plates is notably influenced by both the size of the hole and the plate's slenderness ratio. Furthermore, it was observed that plates with circular perforations generally exhibit a higher ultimate load-bearing capacity compared to those with square perforations. Due to the complexity of this subject and aiming to enhance accessibility and understanding for a broader audience, including students and non-specialists, a Glossary can be found in the final of the article.

3. Computational Model

The present investigation applied the FEM through the commercial software ANSYS® Mechanical APDL. The finite element adopted for the performed thin plate analysis was the SHELL281, which has eight nodes with six degrees of freedom at each node: three rotations around *x*, *y*, and *z*-axes and three translations in *x*, *y*, and *z*-axes (Ansys®, 2024). The selection of this engineering simulation software was due to the accurate results it produced in analyzing the behavior of thin plates under buckling conditions (Baumgardt et al., 2023; da Silveira et al., 2022; Fragassa, Minak, & Pavlovic, 2020; Lima et al., 2020; Pavlovic, Fragassa, & Minak, 2017; Silveira et al., 2021), as well as in other structural engineering problems (Bhadra et al., 2023; Gonenli & Das, 2022; Kucharski et al., 2022; Milošević et al., 2017; Pavlovic & Fragassa, 2020; Safaei et al., 2023; Skripnyak et al., 2021). In the present work,

two computational domains were used: a reference plate (with no hole) and a perforated plate, both simply-supported and submitted to biaxial compressive loading, as represented in Figure 1.

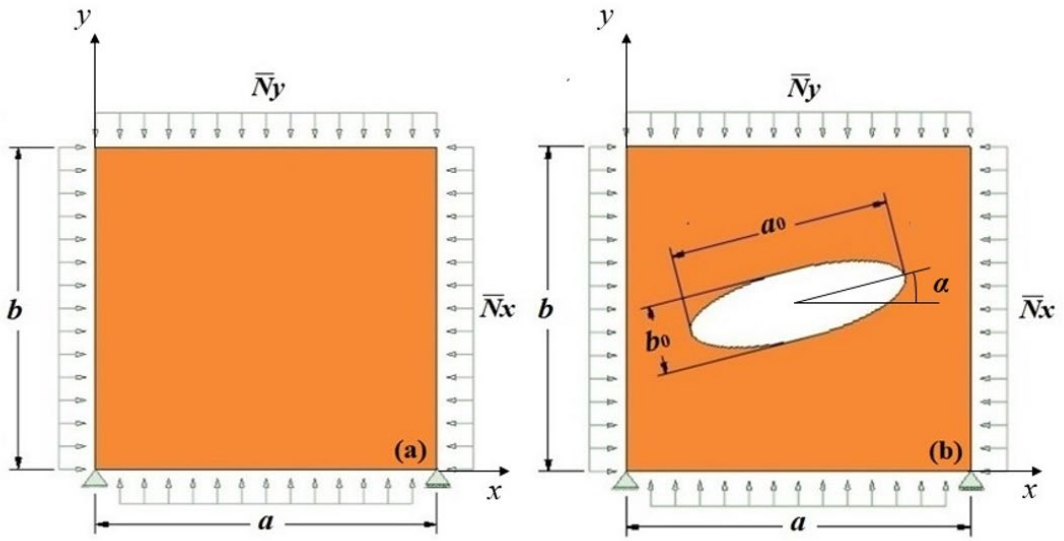

Figure 1. Computational Domain of the Simply-Supported and Biaxially Compressed: (a) Reference Plate and (b) Perforated Plate.

In the numerical simulation of the post-buckling behavior of plates, the analysis assumed an elastic-perfectly plastic material response. As noted by El-Sawy et al., elasto-plastic buckling analysis requires the inclusion of an initial imperfection in the plate, which can be obtained from the first elastic buckling mode, characterized by a maximum displacement w_0, where b is the width of the plate (see Figure 1)(El-Sawy, Nazmy, & Martini, 2004):

$$w_0 = \frac{b}{2000} \tag{1}$$

The ultimate load of the reference and the perforated plates might be obtained by using as reference the yield load, defined as (Lima et al., 2020):

$$P_y = \sigma_y t \tag{2}$$

where σ_y is the yield stress of material; and being P_y incremented gradually over the plate edges in x and y-direction. With each load increment, the Newton-Raphson method is employed to calculate the corresponding displacements that bring the plate to its equilibrium configuration. At the outset of loading step $i + 1$, there is an out-of-balance load vector $\{\psi\}$, equivalent to the load increment $\{\Delta\bar{N}\}$, between the vector of external loads, $\{\bar{N}\}_{i+1}$, and the vector of nonlinear internal forces $\{F_{NL}\}$, which equals the preceding external load vector $\{\bar{N}\}_i$, as follows (Lima et al., 2020):

$$\{\psi\} = \{\Delta\bar{N}\} = \{\bar{N}\}_{i+1} - \{F_{NL}\} = \{\bar{N}\}_{i+1} - \{\bar{N}\}_i \tag{3}$$

Subsequently, the Newton-Raphson method is applied iteratively to minimize the out-of-balance load vector$\{\psi\}$ below a specific tolerance, by using the following equations:

$$\{\psi\}_{r+1} = \{\bar{N}\}_{i+1} - \{F_{NL}\}_r \tag{4}$$

$$\{\psi\}_{r+1} = [K_t]_r\{\Delta U\}_{r+1} \tag{5}$$

$$\{U\}_{r+1} = \{U\}_r + \{\Delta U\}_{r+1} \tag{6}$$

where $\{\psi\}_{r+1}$ represents the updated out-of-balance load vector, $\{F_{NL}\}_r$ is the nonlinear internal forces vector at iteration r, $[K_t]_r$ is the tangent stiffness matrix calculated as a function of the displacement vector $\{U\}_r$, and $\{U\}_{r+1}$ stands for the updated displacement increment vector. Before performing numerical simulations to obtain the results of the present work, verifications and validation steps were conducted to ensure the accuracy of the proposed computational model. Among all realized analyses, six of them can be highlighted. Firstly, two verifications were carried out to certify the accuracy of computational model for biaxial elastic buckling analysis, which is an important

step to the elasto-plastic buckling simulation, once the initial imperfection of plate depends of it's elastic bucking deformation. The first verification for elastic buckling was performed based on Piscopo (Piscopo, 2010). For that, a simply-supported steel plate, without perforation, with a/b = 1, t/b = 0.01, Young's Modulus E = 206 GPa, and Poisson's ratio v = 0.3, was analyzed by analytical and numerical approaches (see Figure 1a). From Piscopo, the analytical solution obtained a critical load of $\bar{N}_{cr}$= 372 N/mm while the computational solution indicates $\bar{N}_{cr}$= 373 N/mm (Piscopo, 2010). Numerically simulating this case, the obtained critical load is $\bar{N}_{cr}$= 368.89 N/mm, representing a difference of 1.1%. Additionaly, based on Jayashankarbabu and Karisiddappa (2014), a perforated steel plate was analyzed through the FEM. For E = 210924 MPa, v = 0.3, b = 1000 mm, and t = 10 mm, the critical load obtained is $\bar{N}_{cr}$ = 314.55 N/mm for a square perforation of $a_0 = b_0$ = 250 mm, and $\bar{N}_{cr}$= 295.48 N/mm for $a_0 = b_0$ = 500 mm (see Figure 1b, only replacing the elliptical hole by a square one with $\alpha = 0°$). For these same cases, with the proposed computational model it was reached $\bar{N}_{cr}$= 314.39 N/mm for perforation of 250 mm and $\bar{N}_{cr}$= 297.49 N/mm for 500 mm. The comparison represents differences of 0.1% and 0.7% for holes with 250 mm and 500 mm, respectively. In turn, the first verification for elasto-plastic buckling was performed based on Shanmugam and Narayanan in which the elasto-plastic buckling was analytically studied for a rectangular steel plate without a hole (Shanmugam & Narayanan, 1998). With yield stress σ_y = 245 MPa, Young's modulus E = 205 GPa, and Poisson's ratio v = 0.30, a simply-supported, rectangular, steel plate was evaluated with a = 720 mm, b = 240 mm, and t = 4 mm (see Figure 1a). The analytical solution resulted in an ultimate stress of σ_u = 56.35 MPa while the proposed computational model obtained σ_u = 56.60 MPa, with 5.1% of difference between them. Another verification of the computational model was made based on Shanmugam et al. (Shanmugam, Thevendran, & Tan, 1999). To do so, a plate with $a = b$ = 125 mm, t = 6.25 mm, circular cutout with $a_0 = b_0$ = 25 mm, boundary conditions as simply-supported, and equal biaxial compressive loads on x and y-directions were considered (see Figure 1b). For the evaluation, the material used in the investigation was AH-36 steel with σ_y = 355 MPa, E = 210 GPa, and v = 0.30. The ultimate stress obtained by the proposed equation of Shanmugam et al. resulted in σ_u = 257.13 MPa, while σ_u = 276.42 MPa was numerically obtained in the present work (Shanmugam, Thevendran, & Tan, 1999). This value represents a difference of 6.98% between numerical and analytical solutions, being acceptable according to Shanmugam et al. (Shanmugam, Thevendran, & Tan, 1999). Moreover, two validations were carried out: the first for a plate without cutout and the second abh 5.77%. The second validation was carried out based on Narayanan and Chow to confirm the computational model accuracy (Narayanan & Chow, 1984). For that, it was considered a simply-supported square plate with $a = b$ = 125 mm and t = 1.625 and with a centered circular hole of $a_0 = b_0$ = 25 mm, under biaxial compressive loading (see Figure 1b). The steel plate analyzed has σ_y = 323.3 MPa, E = 205 GPa, and v = 0.30. The experimental result presented by Narayanan and Chow is σ_u = 73.8 MPa, while the solution obtained by the computational model is σ_u = 77.59 MPa, representing an error of 5.13% (Narayanan & Chow, 1984). Based on relative percentage discrepancies obtained through the verification and validation processes, it is possible to infer that the computational model attends the analysis of the biaxial elasto-plastic buckling of thin steel plates (with or without perforations) with good accuracy. After the verification and validation of the computational model, the numerical simulations of the present work were developed adopting a converged SHELL281 mesh generated by quadrilateral finite elements with 50 mm side and refined at the line around the cutout.

4. Constructal Design Method Application

The Constructal Design (CD) method allows the understanding of the effect of geometric configuration on the system performance. According to Bejan and Zane and Bejan, the Constructal Law is revolutionary because it is a law of physics and governs the design and rhythm of any finite-size flow system, anywhere, encompassing animate (trees and animals), inanimate (rivers and lightning bolts), and engineered (technology) phenomena (Bejan, 2019; Bejan & Peder Zane, 2012). In other words, the Constructal Law can be understood as a unifying principle of design (Rocha et al., 2013). It is important to mention that CD is not an optimization method, being necessary to use it simultaneously with an optimization technique if the goal is to reach a superior performance for the analyzed system (dos Santos et al., 2017). In this work, it is used the Exhaustive Search technique (ES) as the optimization method. It is important to highlight the CD method is widely applied in transport phenomena engineering problems, for instance: Feijó et al., Nunes et al., Zhang et al., Razera et al., Cunegatto et al., Feng et al., Liu et al., Chen et al., Dan et al., Feng et al., Rodha et al., and Lu et al. (Chen et al., 2024; Cunegatto, Gotardo, & Zinani, 2023; Dan et al., 2024; Feijó et al., 2022; Feng et al., 2023; Feng et al., 2024; Liu et al., 2023; Lu et al., 2024; Nunes et al., 2021; Razera et al., 2022; Zhang et al., 2021). However, according to Bejan and Lorente, in Structural Engineering, systems can be conceptualized as flow systems tailored to guide the distribution of stress (Bejan & Lorente, 2008). While interpreting stress as a flow may seem unconventional, it proves useful for determining the optimal geometric configuration of structural components under stress. For each failure mechanism, there are ways to channel stresses to maximize load capacity

within a fixed volume or reduce volume for a given load (Lorente, Lee, & Bejan, 2010). Da Silveira et al. provide further detail on the benefits of Constructal Design (CD) in Structural Engineering (da Silveira et al., 2022). Bejan and Lorente suggest that all flow systems inherently possess imperfections, which cannot be eliminated but can be strategically distributed to ease the flow of currents (Bejan & Lorente, 2008). In Mechanics of Materials, these imperfections manifest as stress concentrations. Thus, achieving superior structural performance relies on distributing maximum allowable stresses uniformly throughout the material. As outlined by Dos Santos et al., applying the Constructal Design (CD) method involves setting constraints (either global or local), defining at least one degree of freedom (to vary within these constraints), and selecting at least one performance indicator for optimization (dos Santos et al., 2017). Within this framework, the current study examines the mechanical behavior of perforated square and rectangular steel plates under biaxial compressive loads of equal magnitude in both in-plane directions, focusing on elasto-plastic buckling behavior. As constraints were considered: the plate volume (V), the plate thickness (t), and the volume fraction (ϕ) which is defined as the ratio between the elliptical perforation volume and the reference plate volume (without hole). As degrees of freedom were considered: the plate's aspect ratio (b/a), the elliptical hole aspect ratio (b_0/a_0), and the hole angular orientation (α). In addition, two performance indicators were used: the Normalized Ultimate Stress (NUS), which should be maximized and is calculated as the ratio of the ultimate stress of the perforated plate (σ_u) and the ultimate stress of the reference plate (σ_{ur}); and for the cases where the same NUS was obtained to more than one b_0/a_0, the Normalized Maximum Deflection (NMD) was also applied, which might be minimized and is defined by the ratio between the maximum deflection obtained for the perforated plate (U_z) and for the reference plate (U_{zr}). Notably, each geometric configuration suggested by the CD method (the search space) was evaluated through numerical simulations—around 700 cases in total—with their results compared to achieve geometric optimization using the Exhaustive Search (ES) technique. Figure 2 provides a simulation tree that defines the search space used by CD, while Figure 3 outlines the steps involved in the application of CD, FEM, and ES for this engineering problem.

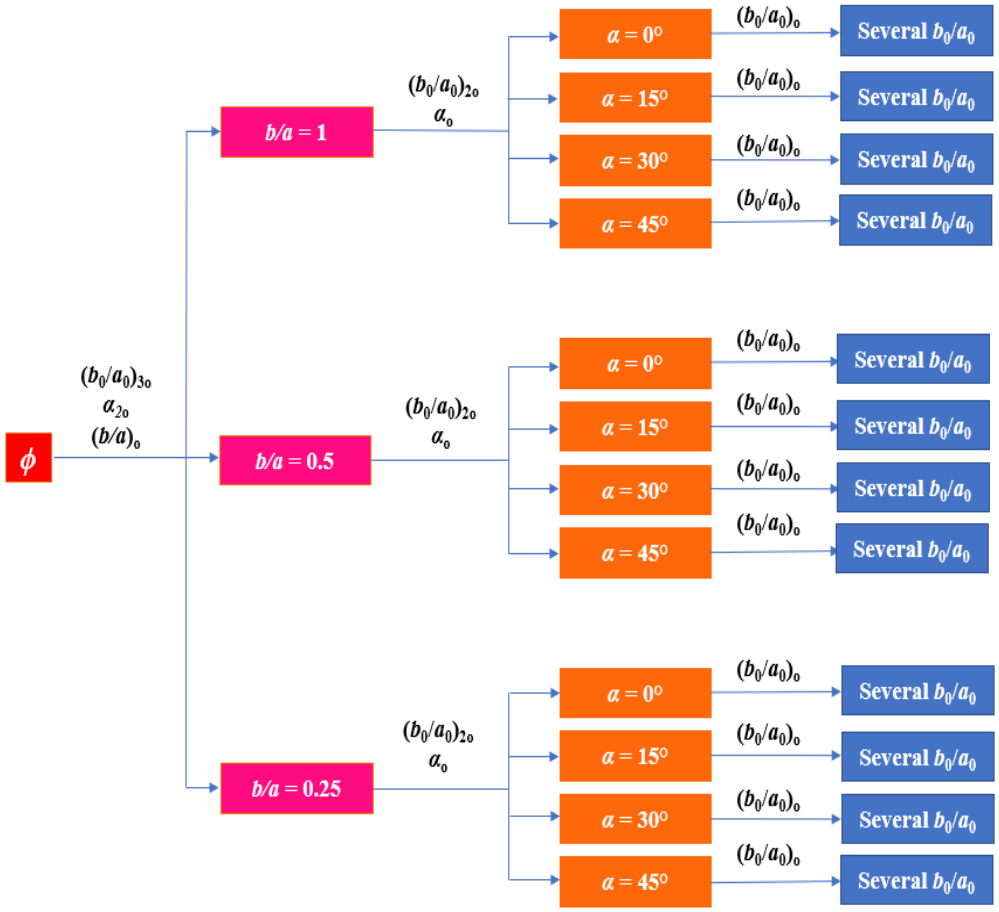

Figure 2. Simulation Tree to Define the Search Space by using Constructal Design.

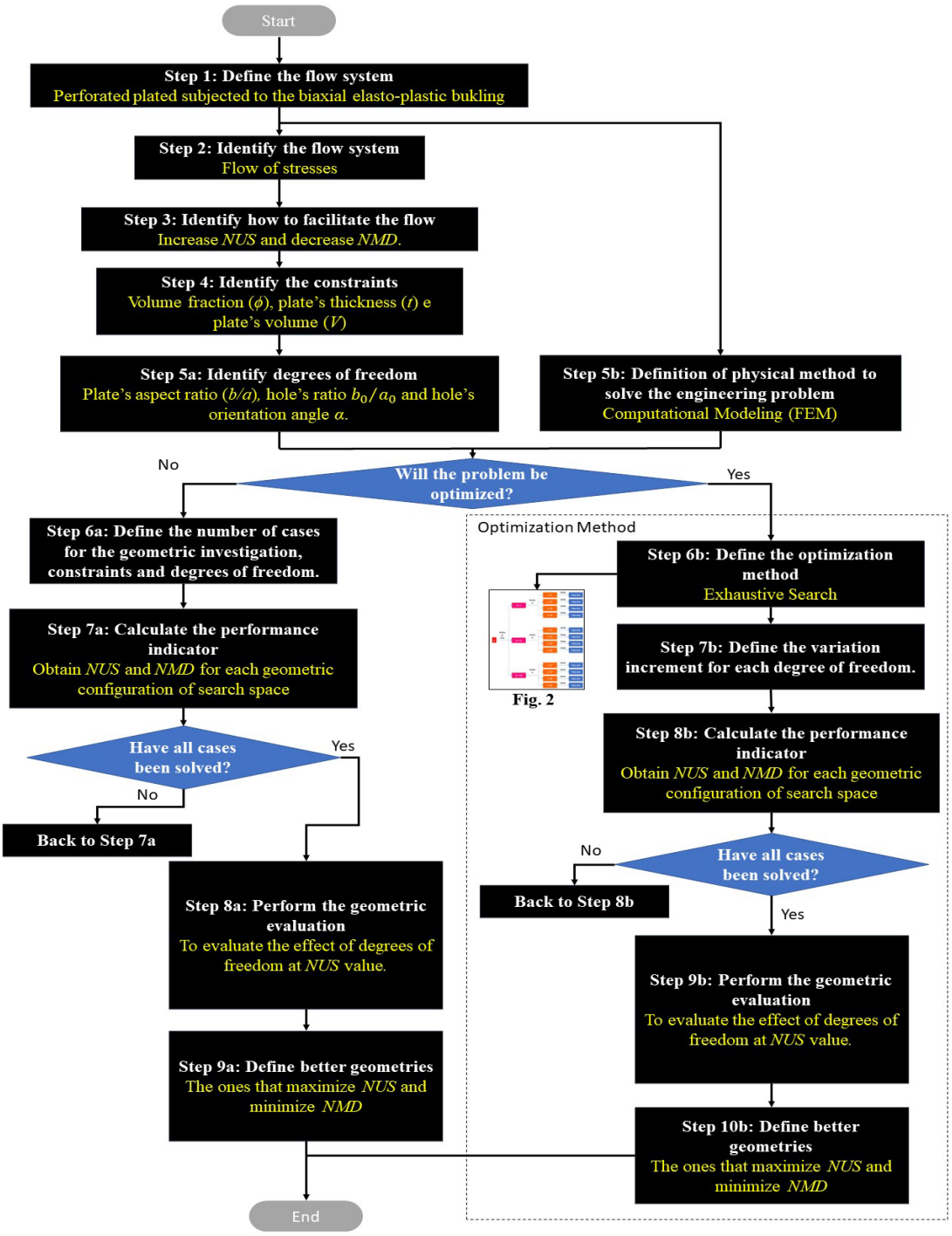

Figure 3. Flowchart of Constructal Design, Finite Element Method, and Exhaustive Search Application in the Geometric Optimization.

5. Results and Discussion

The simply-supported steel plates analyzed are made of AH-36 steel, characterized by the next properties: σ_y = 355 MPa, E = 210 GPa, and ν = 0.30. As shown in Figure 2, three different b/a values were analyzed, maintaining the same thickness t = 12 mm: b/a = 1 (a = b = 1414.214 mm); b/a = 0.5 (a = 2000 mm and b = 1000 mm); and b/a = 0.25 (a = 2828.43 mm and b = 707.11 mm), resulting in the same volume of material for all ratios of b/a. Five different

volume fractions were adopted for the elliptical cutouts: ϕ = 0.025; 0.05; 0.10; 0.15; and 0.20. In addition, four different orientations of cutout were considered for all analyzed perforations: α = 0º; 15º; 30º; and 45º. Varying a_0 and b_0, for all ϕ, the cutout geometry was changed (through the degree of freedom b_0/a_0) keeping constant the volume of removed material. In this section, the obtained curves for the *NUS* variation as a function of the degrees of freedom variations are presented for all volume fractions considering α = 0º. Moreover, von Mises stress distributions are presented for ϕ = 0.05 and α = 0º. In addition, curves from *NUS* analysis and von Mises stress distributions for orientations α = 15º; 30º; and 45º are presented in Appendix A and are considered in discussions of results. Plates were analyzed for all volume fractions ϕ. Several values for the ratio b_0/a_0 were considered, hence varying the dimensions a_0 and b_0 (see Figure 1b) and the cutout's geometry, but maintaining the same volume of removed material by the perforation. All σ_u obtained were used to calculate the *NUS* factor, considering as a reference the ultimate stress σ_{ur} of the no-hole plate (see Figure 1a). When necessary, the maximum deflection U_z obtained from the numerical simulations was used to calculate the *NMD* factor, taking into account the maximum deflection of the no-hole reference plate U_{zr}. Table 1 presents the aspect ratios for the reference plate (see Figure 1), as well as its numerical results for stress and deflection.

Table 1. Reference Values of Stress and Deflection for each Plate's Aspect Ratio.

b/a	σ_{ur} (MPa)	U_{zr} (mm)
1	56.80	44.73
0.5	49.70	39.41
0.25	56.80	11.20

5.1. Square Plates with *b*/*a* = 1

Figure 4 presents the obtained curves for *NUS* varying the degree of freedom b_0/a_0 for all volume fractions and α = 0º. The obtained curves for α = 15º; 30º; and 45º are presented, respectively, in Figs. A.1; A.2; and A.3 in Appendix A.

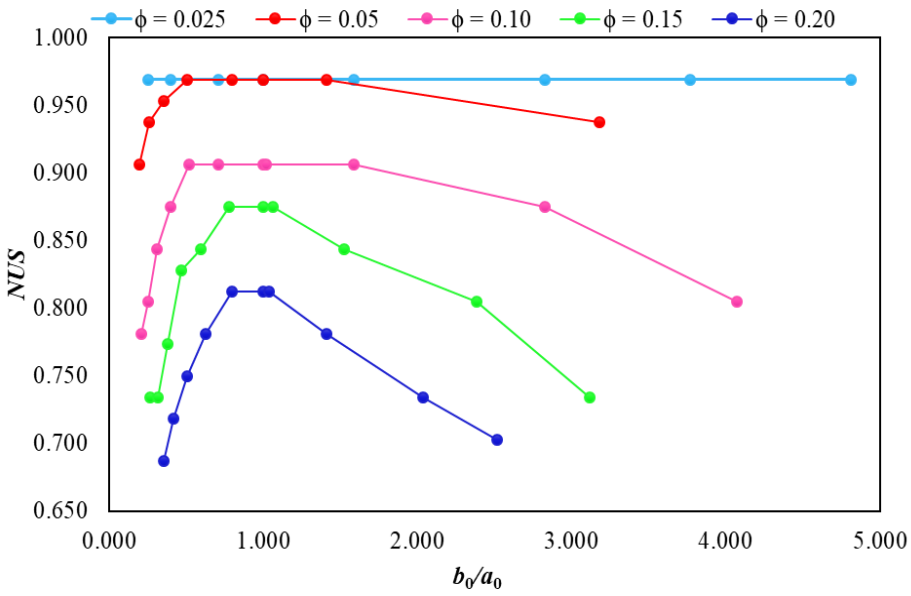

Figure 4. Curves of the *NUS* for the Plates with b/a = 1 and α = 0º.

Based on Figures 4 and A.1 to A.3 it is noticeable that independently of orientation α, the *NUS* factor behavior follows the same pattern, increasing from the smaller values of b_0/a_0 to close to b_0/a_0 = 1.000, and then decreasing as b_0/a_0 increases. In addition, as expected it is possible to infer that the increase in cutout volume fraction directly impacts the mechanical strength of the plate, leading to a reduction in NUS values. For smaller volume fractions, several geometries achieved the maximum *NUS* requiring a second evaluation based on the *NMD* factor. On the other hand, as ϕ increases, the quantity of geometries with maximized *NUS* decreased making necessary the *NMD* evaluation for a smaller quantity of cases. As the maximized *NUS* was obtained for more than one b_0/a_0, the consideration of the *NMD* factor was needed to obtain the geometry once optimized for each α. It was observed that for all square plates

(b/a = 1) the geometry, once optimized, with maximized *NUS* and minimized *NMD* is the circular hole $(b_0/a_0)_o$ = 1.000. As for the circular hole the orientation α is not effective, the geometry twice optimized for square plates and for all ϕ values, is $(b_0/a_0)_{2o}$ = 1.000. Table 2 presents the best results for each volume fraction and Figure 5 depicts the von Mises stress distributions for the square plates with ϕ = 0.05.

Table 2. Optimizations in First and Second Levels for each Volume Fraction and b/a = 1.

ϕ	α	$(b_0/a_0)_o$	NUS_m	$(b_0/a_0)_{2o}$	NUS_{2m}	NUS_{min}	α_o
0.025	0°	1.000	0.969	1.000	0.969	0.969	-
	15°	1.000	0.969				
	30°	1.000	0.969				
	45°	1.000	0.969				
0.05	0°	1.000	0.969	1.000	0.969	0.906	-
	15°	1.000	0.969				
	30°	1.000	0.969				
	45°	1.000	0.969				
0.10	0°	1.000	0.906	1.000	0.906	0.781	-
	15°	1.000	0.906				
	30°	1.000	0.906				
	45°	1.000	0.906				
0.15	0°	1.000	0.875	1.000	0.875	0.734	-
	15°	1.000	0.875				
	30°	1.000	0.875				
	45°	1.000	0.875				
0.20	0°	1.000	0.813	1.000	0.813	0.688	-
	15°	1.000	0.813				
	30°	1.000	0.813				
	45°	1.000	0.813				

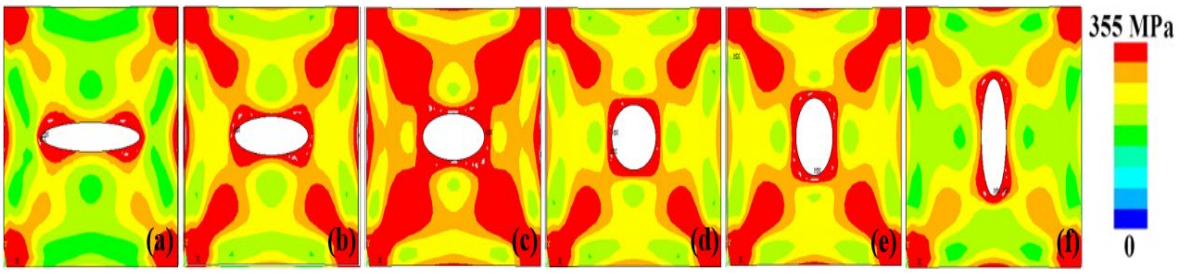

Figure 5. Distribution of Von Mises Stresses for the Plates with b/a = 1, ϕ = 0.05, and α = 0°, being: (a) b_0/a_0 = 0.199; (b) b_0/a_0 = 0.354; (c) b_0/a_0 = 0.509; (d) $(b_0/a_0)_{2o}$ = 1.000; (e) b_0/a_0 = 1.415; and (f) b_0/a_0 = 3.183.

From Figure 5, it is noticeable the difference on von Mises stresses among the plates due to cutout variation. To evaluate the stress distributions, the Constructal Principle of Optimal Distribution of Imperfections (PODI) was applied, with the imperfections in Mechanics of Materials problems represented by the maximum stress concentrations (Bejan and Lorente, 2008). The geometries (c), (d), and (e) of Figure 5 are the ones that achieved the higher values for the *NUS* factor. For these von Mises stress distributions, it is worth mentioning the bigger quantity of areas submitted to the maximum stresses (represented by red color) if compared to the cases (a), (b), and (f) of Figure 5, which reached the worst mechanical behavior. Among the plates with the best performance, the perforation of $(b_0/a_0)_{2o}$ = 1.000 is the one that provides the best distribution of stresses since a symmetric distribution of von Mises stresses was provided. The same behavior can be observed in Figures B.1 to B.3 in Appendix B, where the circular hole is the one that conducts to the superior performance.

5.2. Rectangular Plates with b/a = 0.5

Considering b/a = 0.5 and observing the references values in Table 1, it is worth mentioning that occurs a reduction of 12.5% in the plate strength if compared with the square plate (b/a = 1) and the same occurs to the deflection, which is 11.89% inferior to that obtained for the reference square plate. Figure 6 presents the generated curves due to the *NUS* variation according to the several b_0/a_0 ratio values for all volume fractions and α = 0º. The analogous curves for α = 15º; 30º; and 45º are plotted, respectively, in Figures. A.4; A.5; and A.6 of Appendix A.

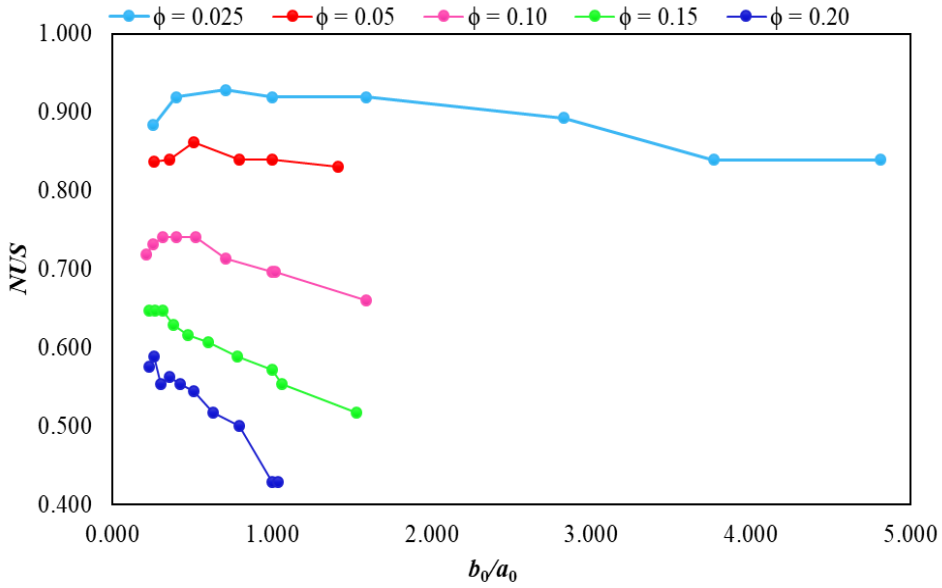

Figure 6. Curves of the *NUS* for the Plates with $b/a = 0.5$ and $\alpha = 0°$.

Based on Figure 6 and Figures A.4 to A.6 (see appendix A), one can observe that for $b/a = 0.5$, the plate mechanical behavior is better, in a general way, for the geometric configurations with $b_0/a_0 \leq 1.000$ and inclination angle $\alpha = 0º$. However, in cases having $b_0/a_0 > 1.000$, the inclination angle $\alpha = 45º$ conducts to the best mechanical performance. Moreover, for the volume fractions (ϕ) analyzed, it is possible to infer that the mechanical behavior is directly affected by the increasing of removed material volumes, occurring as expected a reduction of the *NUS* factor as ϕ increases. Still considering Figures 6 and A.4 to A.6, for the cases in which the same maximized *NUS* magnitude was achieved for more than one b_0/a_0 value, the consideration of *NMD* factor was needed to obtain the geometry once optimized for each α. Therefore, the results showed different optimized geometries for each volume fraction analyzed. The best results of each volume fraction, considering inclination angles and two optimizations, are presented in Table 3. Besides that, Figure 7 depicts the distribution of von Mises stresses for rectangular plates with $b/a = 0.5$, $\phi = 0.05$, and $\alpha = 0º$. Regarding the results of Figure 7, it can be observed the influence of cutout in the von Mises stress distribution on these rectangular steel plates. The twice-optimized geometry presented in Figure 7c is responsible for the best plate performance. Comparing this geometry defined by $(b_0/a_0)_{2o} = 0.509$ with the others, one can note that the superior mechanical behavior was obtained by the plate that has the greater area of maximum stresses (imperfections of the system), represented by red color. It means that the plate of Figure 7c, which reached the $NUS_{2m} = 0.862$, is in line with the PODI (Bejan & Lorente, 2008). The same behavior can be seen in Figures B.4 to B.6 (see appendix B), where different inclination angles are considered for the distribution of von Mises stresses; as well as in previous works addressed to similar structural engineering applications, such as Helbig et al. and Lima et al.(Helbig et al., 2016; Lima et al., 2020).

Table 3(a). Optimizations in First and Second Levels for each Volume Fraction and $b/a = 0.5$.

ϕ	α	$(b_0/a_0)_o$	NUS_m	$(b_0/a_0)_{2o}$	NUS_{2m}	NUS_{min}	α_o
0.025	0°	0.707	0.929	0.707	0.929	0.839	0°
	15°	0.707	0.929				
	30°	0.707	0.929				
	45°	1.592	0.929				
0.05	0°	0.509	0.862	0.509	0.862	0.732	0°
	15°	0.796	0.857				
	30°	0.796	0.839				
	45°	1.000	0.839				
0.10	0°	0.314	0.741	0.314	0.741	0.571	0°
	15°	0.520	0.732				
	30°	0.707	0.696				
	45°	1.000	0.696				

Table 3(b). Optimizations in First and Second Levels for each Volume Fraction and $b/a = 0.5$.

ϕ	α	$(b_0/a_0)_o$	NUS_m	$(b_0/a_0)_{2o}$	NUS_{2m}	NUS_{min}	α_o
0.15	0°	0.226	0.647	0.226	0.647	0.464	0°
	15°	0.382	0.616				
	30°	0.597	0.589				
	45°	1.000	0.571				
0.20	0°	0.260	0.589	0.260	0.589	0.375	0°
	15°	0.421	0.518				
	30°	0.629	0.464				
	45°	2.037	0.429				

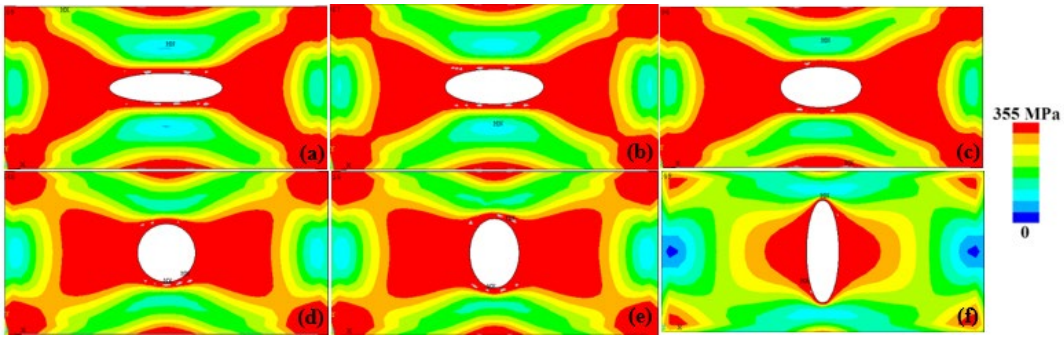

Figure 7. Distribution of von Mises stresses for the plates with $b/a = 0.5$, $\phi = 0.05$, and $\alpha = 0°$, being: (a) $b_0/a_0 = 0.260$; (b) $b_0/a_0 = 0.354$; (c) $(b_0/a_0)_{2o} = 0.509$; (d) $b_0/a_0 = 1.000$; (e) $b_0/a_0 = 1.415$; and (f) $b_0/a_0 = 3.183$.

5.3. Rectangular Plates with $b/a = 0.25$

The third analysis group is related to rectangular plates having $b/a = 0.25$, with dimensions and properties earlier described, and that were analyzed for the five proposed values of volume fractions ϕ. Through Table 1, it is noticeable that the σ_{ur} is the same obtained result for $b/a = 1$. Although the ultimate stress is the same that for a square plate, it is essential to note that when considering the maximum deflection U_{zr} for both cases, the square plate has a deflection 299.4% bigger than the one obtained for $b/a = 0.25$. Figure 8 presents the generated curves for *NUS* varying the degree of freedom b_0/a_0 for all volume fractions and $\alpha = 0°$. The obtained curves for $\alpha = 15°$; 30°; and 45° are presented, respectively, in Figures A.7; A.8; and A.9 (Appendix A).

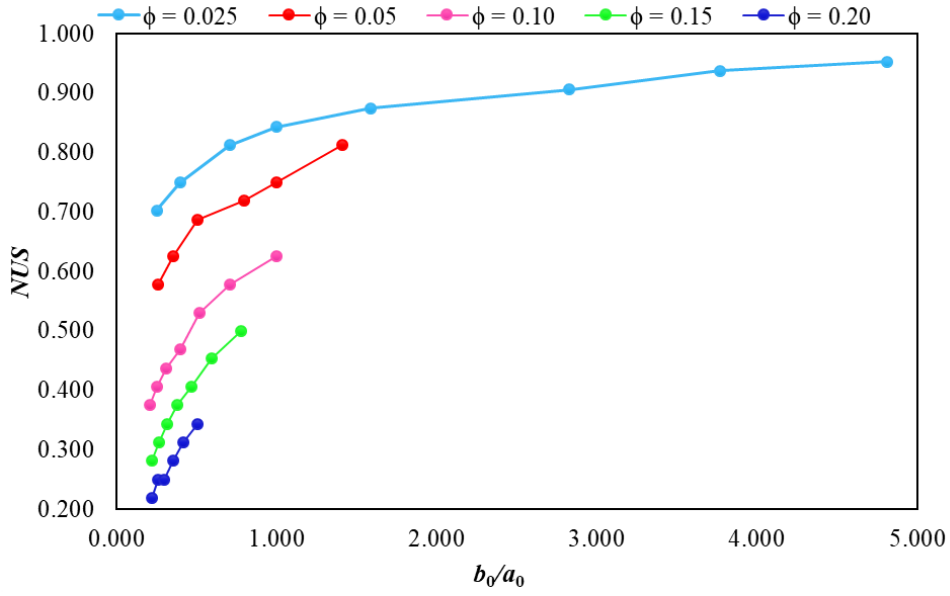

Figure 8. Curves of the *NUS* for the Plates with $b/a = 0.25$ and $\alpha = 0°$.

Figures 8 and A.7 to A.9 indicate that the increasing volume fraction ϕ causes a worsening of mechanical behavior, as already observed in $b/a = 1$ and 0.5. Especially for the cases considering $\alpha = 45º$, for the tested cutouts, the geometry variation is not effective in changing the mechanical behavior. What can be noted, as characteristics for these analyses, is that for the major part of optimized geometric configurations and all twice-optimized geometries, the best performance is achieved for bigger values of b_0/a_0, i.e., the best mechanical behaviors are reached as longer is the hole geometry in the y-direction. Figure 9 illustrates the von Mises stress distributions for the plates with $b/a = 0.25$, $\phi = 0.05$, and $\alpha = 0º$. In Appendix B, Figures B.7 to B.9 illustrate the same analysis for different inclination angles. Assitionaly, Table 4 presents the best results considering inclination angles and two optimization levels. When compared to the general behavior of plates for the three aspect ratios (b/a) analyzed, $b/a = 0.25$ presents a different behavior considering its optimal geometries. From Figures 9 and B.7 to B.9 can be observed that, for this aspect ratio, plates present smaller areas submitted to the maximum stresses (represented by red color), and these areas are concentrated around the cutout, as can be seen in Figure 9d for the twice-optimized geometry $(b_0/a_0)_{2o} = 1.415$ with $b/a = 0.25$, $\phi = 0.05$, and $\alpha = 0°$. On the other hand, the major area of the plate is subjected to smaller stresses or even null stresses (represented by blue color), as can be seen in Figure B.7d for $(b_0/a_0)_o = 1.415$. Based on these observations, it can be affirmed that for $b/a = 0.25$ the mechanical behavior is defined, basically, by the distribution of stresses around the cutout. This finding can be explained based on the flow of stresses by elasto-plastic buckling, which can be more or less affected by the cutout geometry. Considering the dimension in the x-direction is four times bigger than the y-direction, for $b/a = 0.25$, stresses in the y-direction are considerably larger than the stresses in the x-direction, meaning that the optimal geometries will be the ones that provide the best flow of stresses in the y-direction, i.e., in the direction of the most representative stresses in the system. This observation and the results of the optimized geometric configuration agree with the Constructal PODI (Bejan & Lorente, 2008).

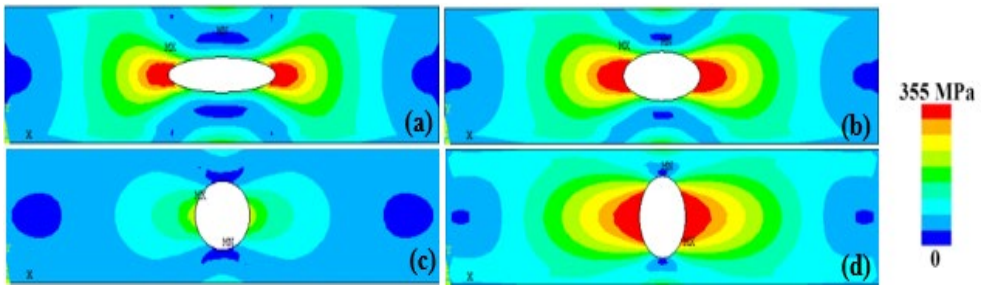

Figure 9. Distribution of Von Mises Stresses for the Plates with $b/a = 0.25$, $\phi = 0.05$, and $\alpha = 0°$, being: (a) $b_0/a_0 = 0.260$; (b) $b_0/a_0 = 0.509$; (c) $b_0/a_0 = 1.000$; and (d) $(b_0/a_0)_{2o} = 1.415$.

Table 4. Optimizations in First and Second Levels for each Volume Fraction and $b/a = 0.25$.

ϕ	α	$(b_0/a_0)_o$	NUS_m	$(b_0/a_0)_{2o}$	NUS_{2m}	NUS_{min}	α_o
0.025	0°	4.814	0.953	4.814	0.953	0.703	0°
	15°	4.814	0.938				
	30°	4.814	0.906				
	45°	1.000	0.844				
0.05	0°	1.415	0.813	1.415	0.813	0.578	0°
	15°	1.415	0.781				
	30°	1.415	0.781				
	45°	0.260	0.781				
0.10	0°	1.000	0.625	1.592	0.688	0.250	30°
	15°	1.000	0.625				
	30°	1.592	0.688				
	45°	0.520	0.625				
0.15	0°	0.780	0.500	0.780	0.500	0.219	30°
	15°	0.780	0.500				
	30°	0.780	0.500				
	45°	0.780	0.438				
0.20	0°	0.509	0.344	0.629	0.375	0.219	15°
	15°	0.629	0.375				
	30°	-	-				
	45°	-	-				

5.4. Global Comparison

Through the comparison among obtained results for the three investigated b/a values, considering all proposed inclination angles α, all studied volume fractions ϕ, and all analyzed degrees of freedom b_0/a_0, it can be achieved the third level of optimization of this study. Figure 10 presents the distribution of von Mises stresses for the three times optimized geometries for each volume fraction ϕ.

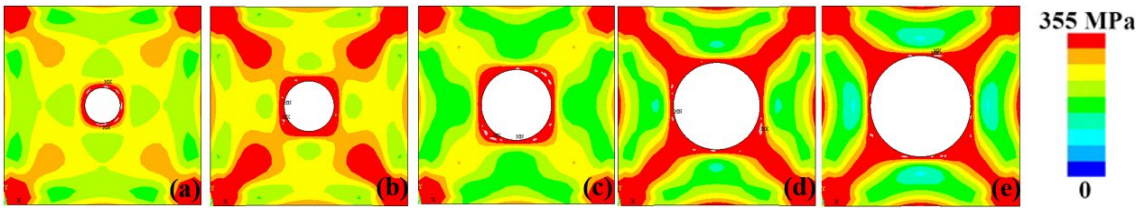

Figure 10. Distribution of von Mises stresses at the third optimized geometry for (a) $\phi = 0.025$; (b) $\phi = 0.05$; (c) $\phi = 0.10$; (d) $\phi = 0.15$; and (e) $\phi = 0.20$.

Figure 10 illustrates that for all volume fractions, the same degree of freedom was obtained, being the circular hole, the geometry three times optimized, $(b_0/a_0)_{3o} = 1.000$. The optimized aspect ratio b/a is the one that conducts to the square plate $(b/a)_o = 1$. Once the circular hole is the three times optimized geometry, while the inclination angle twice optimized, α_{2o}, does not affect the results. Examples of circular holes application in real-world engineering structures can be observed in Figure 11.

Figure 11. Application of Circular and Elliptical Holes in Engineering Structures.

Figure 11 illustrates some images from oil and gas, aeronautical, and naval structures. One can observe circular holes in a drillsihip, in internal reinforcements of an aircraft wing, and in ship hulls, as well as elliptical cutouts used as airplane windows. Therefore, it is evident that this type of perforation is applicable to a broad range of real-world scenarios in structural engineering, emphasizing the importance of understanding the mechanical behavior of perforated plates under buckling conditions.

6. Conclusions

Understanding the behavior of thin steel plates is crucial, as these structural components are used in many engineering applications. The approach to elasto-plastic buckling is particularly important when designing lighter structures with higher mechanical strength, as this phenomenon allows for an increased load capacity compared to elastic buckling. The Finite Element Method (FEM), combined with Constructal Design (CD) and Exhaustive Search Technique (ES), was adopted to optimize the geometries of perforated plates with a centered elliptical cutout to

achieve the best structural performance under biaxial compressive loads, up to elasto-plastic buckling. This approach to such real-world Structural Engineering problems represents an original scientific contribution of this research. Through the analysis of the aspect ratio b/a for the plates, it was possible to observe that the variation of b/a affects directly the mechanical behavior of the plate. Among the analyzed reference plates (without cutouts), the best performance was achieved with $b/a = 0.25$. When considering b/a values of 0.25 and 1, the ultimate stress obtained was the same, being 14.3% higher than for $b/a = 0.5$. Additionally, regarding plate deflections, the plate with $b/a = 0.25$ is the best option among those without holes. For maximum deflections, the plate with $b/a = 1$ had deflections 13.5% and 229.4% greater than those for $b/a = 0.25$, respectively. In the case of perforated plates, a change in mechanical behavior was also noted with varying b/a, particularly for $b/a = 0.25$, where maximum stresses are concentrated around the cutout, and the majority of the plate area experiences low or negligible stresses. Analyzing stress components in the x-direction and y-direction revealed that for $b/a = 0.25$, stresses in the y-direction are significantly greater than those in the x-direction. This is a consequence of the resultant load applied at the boundaries, which changes with the values of a and b. Regarding the mechanical strength of perforated plates, as expected, the presence of a cutout reduces the Normalized Ultimate Stress (*NUS*) compared to the reference plate (without a hole). The reduction in *NUS* increases with the volume fraction ϕ. Reductions of up to 18.7%, 41.1%, and 62.5% were observed for $b/a = 1$, 0.5, and 0.25, respectively, for $\phi = 0.20$. For each volume fraction (ϕ) and aspect ratio (b/a), optimizations were performed obtaining geometries twice-optimized and their respective inclination angles once-optimized. A third analysis was conducted, resulting in a geometry three times optimized with the inclination angle twice-optimized and the optimal aspect ratio. It was concluded that, for plates with the same material volume and thickness, the variation in aspect ratio leads to an optimal $(b/a)_o = 1$, which corresponds to a square plate, for all volume fractions ϕ. The three times optimized geometry is $(b_0/a_0)_{3o} = 1.000$ indicating that the circular hole provides the best performance among all analyzed geometries. Since the circular hole is the three times optimized geometry, it means that the inclination angle twice-optimized does not affect this case. On the other hand, for practical applications, the use of rectangular plates can be required. For that, different values of b_0/a_0 can conduct to results twice optimized, which are dependent on α and b/a, as an example: $(b_0/a_0)_{2o} = 0.260$ for $b/a = 0.5$, $\phi = 0.20$, and $\alpha_o = 30°$, which represents an increasing of 37.3% when compared to the circular hole. As illustrated in Figure 11, in engineering structures the most varied applications for the use of steel plates with elliptical and mainly circular perforations are found in practice. Civil, naval, offshore, aerospace, and automotive engineering, among others, widely employ this type of cutout in real-world design solutions, justifying the relevance of its study.

In summary, the main finding that emerge from the present work are: i) The development of a verified and validated FEM computational model to numerically simulate the biaxial elasto-plastic buckling of metal plates with or without perforations; ii) The development of a methodology combining FEM, CD, and ES, which not only determines the optimized geometric configuration of the investigated structural problem but also identifies how geometric variations influence the considered performance indicator; iii) Understanding the elasto-plastic buckling of thin steel plates is essential, particularly for the design of lighter structures with higher mechanical strength, as it allows for increased load capacity compared to elastic buckling; iv) The aspect ratio b/a has a significant impact on the mechanical behavior of plates: for plates without cutouts, the best performance was observed at $b/a = 0.25$, achieving the highest ultimate stress and minimized deflections; v) As expected, the presence of perforations in the plate reduces its ultimate buckling stress capacity; and vi) In general, circular holes lead to superior mechanical performance for perforated plates under biaxial elasto-plastic buckling, but in certain cases of rectangular plates ($b/a < 1$), elliptical holes achieved better mechanical performance than circular ones. In future works it is recommended to apply the methodology developed in the present work to investigate other types of perforations (such as rectangular, oblong, and hexagonal), as well as to take into account the presence of a lateral pressure incidng over the plate in addition to the baiaxial compressive load.

Acknowledgement

The authors L. A. O. Rocha, E. D. dos Santos, and L. A. Isoldi thank to the National Council of Scientific and Technological Development (CNPq) for the research grant (Processes: 307791/2019-0, 308396/2021-9, and 309648/2021-1, respectively). L. A. O. Rocha thanks to Foundation for Science and Technology, I.P. (doi.org/10.54499/UIDP/04683/2020; doi.org/10.54499/UIDB/04683/2020).

References

Åesson, B. (2014). *Plate buckling in bridges and other structures*. CRC Press. https://doi.org/10.1201/9781482266030

Baumgardt, G. R., Fragassa, C., Rocha, L. A. O., dos Santos, E. D., da Silveira, T., & Isoldi, L. A. (2023).

Computational model verification and validation of elastoplastic buckling due to combined loads of thin plates. *Metals*, *13*(4), 731. https://doi.org/10.3390/met13040731

Bejan, A. (2019). *Freedom and evolution: hierarchy in nature, society and science*. Springer Nature. https://doi.org/10.1007/978-3-030-34009-4

Bejan, A., & Lorente, S. (2008). *Design with constructal theory*. John Wiley & Sons. https://doi.org/10.1002/9780470432709

Bejan, A., & Peder Zane, J. (2012). Design in nature. *Mechanical Engineering*, *134*(06), 42-47. https://doi.org/10.1115/1.2012-JUN-4

Bhadra, R., Jana, T., Mitra, A., & Sahoo, P. (2023). Effect of CNT radius on flattening contact behaviour of CNT-Al nanocomposite: A numerical approch. *Reports in Mechanical Engineering*, *4*(1), 121-130. https://doi.org/10.31181/rme040102082023b

Cao, Y., Zhou, Y., Tian, S., Takagi, J., Li, Z., Fang, D., & Fang, X. (2024). Performance of novel perforated double-core steel-plate assembled buckling-restrained braces. *Journal of Building Engineering*, *82*, 108326. https://doi.org/10.1016/j.jobe.2023.108326

Chajes, A. (1974). Principles of structural stability theory. *Prentice-Hall google schola*, *4*, 11-20. https://doi.org/https://books.google.com.pk/books/about/Principles_of_structural_stability_theor.html?id=FeYeAQAAIAAJ&redir_esc=y

Chen, L., Feng, H., Zhang, F., & Ge, Y. (2024). Constructal design for composite heat dissipating structure composed of an “arrow”-shaped high conductivity channel and an externally connected “T”-shaped fin. *International Communications in Heat and Mass Transfer*, *153*, 107341. https://doi.org/10.1016/j.icheatmasstransfer.2024.107341

Cheng, B., & Zhao, J. (2010). Strengthening of perforated plates under uniaxial compression: Buckling analysis. *Thin-Walled Structures*, *48*(12), 905-914. https://doi.org/10.1016/j.tws.2010.06.001

Cunegatto, E. H. T., Gotardo, M., & Zinani, F. S. F. (2023). Numerical analysis of tube arrangements with one, two, and four degrees of freedom for heat transfer with pseudoplastic fluids. *International Journal of Heat and Mass Transfer*, *208*, 124080. https://doi.org/10.1016/j.ijheatmasstransfer.2023.124080

da Silva, C. C. C., Helbig, D., Cunha, M. L., dos Santos, E. D., Rocha, L. A. O., Real, M. d. V., & Isoldi, L. A. (2019). Numerical buckling analysis of thin steel plates with centered hexagonal perforation through constructal design method. *Journal of the Brazilian Society of Mechanical Sciences and Engineering*, *41*, 1-18. https://doi.org/10.1007/s40430-019-1815-7

da Silveira, T., Baumgardt, G., Rocha, L., dos Santos, E., & Isoldi, L. (2022). Numerical simulation and constructal design applied to biaxial elastic buckling of plates of composite material used in naval structures. *Composite Structures*, *290*, 115503. https://doi.org/10.1016/j.compstruct.2022.115503

Dan, Z., Feng, H., Chen, L., Liao, N., & Ge, Y. (2024). Constructal design of printed circuit recuperator for S-CO2 cycle via multi-objective optimization algorithm. *Science China Technological Sciences*, *67*(1), 285-294. https://doi.org/10.1007/s11431-023-2500-x

Dong, J., Ma, X., Zhuge, Y., & Mills, J. E. (2018). Local buckling of thin plate on tensionless elastic foundations under interactive uniaxial compression and shear. *Theoretical and Applied Mechanics Letters*, *8*(2), 75-82. https://doi.org/10.1016/j.taml.2018.02.003

dos Santos, E. D., Isoldi, L. A., Gomes, M. d. N., & Rocha, L. A. (2017). The constructal design applied to renewable energy systems. In *Sustainable energy technologies* (pp. 45-62). CRC Press. https://doi.org/10.1201/9781315269979-4

Ehsani, A., & Dalir, H. (2019). Multi-objective optimization of composite angle grid plates for maximum buckling load and minimum weight using genetic algorithms and neural networks. *Composite Structures*, *229*, 111450. https://doi.org/10.1016/j.compstruct.2019.111450

El-Sawy, K. M., & Martini, M. I. (2010). Stability of biaxially loaded square plates with single central holes. *Ships and Offshore Structures*, *5*(4), 283-293. https://doi.org/10.1080/17445300903566181

El-Sawy, K. M., Nazmy, A. S., & Martini, M. I. (2004). Elasto-plastic buckling of perforated plates under uniaxial

compression. *Thin-Walled Structures*, *42*(8), 1083-1101. https://doi.org/10.1016/j.tws.2004.03.002

Falkowicz, K., & Debski, H. (2021). Stability analysis of thin-walled composite plate in unsymmetrical configuration subjected to axial load. *Thin-Walled Structures*, *158*, 107203. https://doi.org/10.1016/j.tws.2020.107203

Farajpour, M., Shahidi, A., & Farajpour, A. (2018). A nonlocal continuum model for the biaxial buckling analysis of composite nanoplates with shape memory alloy nanowires. *Materials Research Express*, *5*(3), 035026. https://doi.org/10.1088/2053-1591/aab3a9

Feijó, B. C., Pavlovic, A., Rocha, L. A. O., Isoldi, L. A., Lorente, S., & dos Santos, E. D. (2022). Geometrical investigation of microchannel with two trapezoidal blocks subjected to laminar convective flows with and without boiling. *Reports in Mechanical Engineering*, *3*(1), 20-36. https://doi.org/10.31181/rme200103020f

Feng, H., Sun, K., Chen, L., & Ge, Y. (2023). Constructal design of a nanofluid cooling channel with sidewall ribs and cavities in a rectangular heat generation body. *Case Studies in Thermal Engineering*, *41*, 102640. https://doi.org/10.1016/j.csite.2022.102640

Feng, H., Zhang, Z., Chen, L., & Ge, Y. (2024). Constructal design for H-shaped compound heat transfer path in a rectangular heat generation body. *International Journal of Heat and Mass Transfer*, *225*, 125442. https://doi.org/10.1016/j.ijheatmasstransfer.2024.125442

Figueiredo, J., Simões, F., & da Costa, A. P. (2024). Unilateral buckling of thin plates by complementarity eigenvalue analyses. *Thin-Walled Structures*, *205*, 112387. https://doi.org/10.1016/j.tws.2024.112387

Fragassa, C., Minak, G., & Pavlovic, A. (2020). Measuring deformations in the telescopic boom under static and dynamic load conditions. *Facta Universitatis, Series: Mechanical Engineering*, *18*(2), 315-328. https://doi.org/10.22190/FUME181201001F

Ghorbanhosseini, S., Yaghoubi, S., & Bahrambeigi, M. R. (2021). A Comprehensive Study on the Effects of the Boundary Conditions on the Elastic Buckling Capacity of a Perforated Plate. *International Journal of Advanced Design & Manufacturing Technology*, *14*(3). https://doi.org/10.30495/admt.2021.1914605.1227

Gonenli, C., & Das, O. (2022). Free vibration analysis of circular and annular thin plates based on crack characteristics. *Reports in Mechanical Engineering*, *3*(1), 158-167. https://doi.org/10.31181/rme20016032022g

Gore, R., & Lokavarapu, B. R. (2022). Effect of Elliptical Cutout on Buckling Load for Isotropic Thin Plate. In *Innovations in Mechanical Engineering: Select Proceedings of ICIME 2021* (pp. 51-69). Springer. https://doi.org/10.1007/978-981-16-7282-8_5

Guo, Y., & Yao, X. (2021). Buckling behavior and effective width design method for thin plates with holes under stress gradient. *Mathematical Problems in Engineering*, *2021*(1), 5550749. https://doi.org/10.1155/2021/5550749

Helbig, D., Silva, C. C. C. d., Real, M. d. V., Santos, E. D. d., Isoldi, L. A., & Rocha, L. A. O. (2016). Study about buckling phenomenon in perforated thin steel plates employing computational modeling and constructal design method. *Latin American Journal of Solids and Structures*, *13*(10), 1912-1936. https://doi.org/10.1590/1679-78252893

Hou, J., Guo, L., & Yan, J. (2021). Steel plate–restraining panel interaction behavior in buckling-restrained steel plate shear walls. *Thin-Walled Structures*, *169*, 108348. https://doi.org/10.1016/j.tws.2021.108348

Hu, H.-S., Fang, P.-P., Liu, Y., Guo, Z.-X., & Shahrooz, B. M. (2020). Local buckling of steel plates in composite members with tie bars under axial compression. *Engineering Structures*, *205*, 110097. https://doi.org/10.1016/j.engstruct.2019.110097

Ipek, C., Sofiyev, A., Fantuzzi, N., & Efendiyeva, S. P. (2023). Buckling Behavior of Nanocomposite Plates with Functionally Graded Properties under Compressive Loads in Elastic and Thermal Environments. *Journal of Applied and Computational Mechanics*, *9*(4), 974-986. https://doi.org/10.22055/jacm.2023.43091.4019

Jin, Q., Leng, L., & Yang, S. (2024). Buckling analysis of composite plates surface bonded with graphene-reinforced piezoelectric actuators. *Polymer Composites*, *45*(2), 1793-1809. https://doi.org/10.1002/pc.27890

Jones, R. M. (2006). *Buckling of bars, plates, and shells*. Bull Ridge Corporation. https://books.google.com.pk/books?hl=en&lr=&id=UzVBr8b_jS8C&oi=fnd&pg=PR19&dq=Jones,+R.+M.+(2006).+Buckling+of+bars,+plates+and+shells.+Blacksburg:+Bull+Ridge+Publishing.&ots=Vu6-cpiJHM&sig=FKzPDWkPCL3k4T3agRIitvdM8iU&redir_esc=y#v=onepage&q&f=false

Kaveh, A., Dadras, A., & Geran Malek, N. (2019). Optimum stacking sequence design of composite laminates for maximum buckling load capacity using parameter-less optimization algorithms. *Engineering with Computers*, *35*, 813-832. https://doi.org/10.1007/s00366-018-0634-2

Kaveh, A., Dadras, A., & Malek, N. G. (2018). Buckling load of laminated composite plates using three variants of the biogeography-based optimization algorithm. *Acta Mechanica*, *229*, 1551-1566. https://doi.org/10.1007/s00707-017-2068-0

Kucharski, D. M., Pinto, V. T., Rocha, L. A., Dos Santos, E. D., Fragassa, C., & Isoldi, L. A. (2022). Geometric analysis by constructal design of stiffened steel plates under bending with transverse I-shaped or T-shaped stiffeners. *Facta Universitatis, Series: Mechanical Engineering*, *20*(3), 617-632. https://doi.org/10.22190/FUME211016070K

Liang, K., & Yin, Z. (2023). Investigation on nonlinear buckling performance of the optimized wing structure under the realistic flight cases. *Aerospace Science and Technology*, *139*, 108416. https://doi.org/10.1016/j.ast.2023.108416

Lima, J. P. S., Cunha, M. L., dos Santos, E. D., Rocha, L. A. O., de Vasconcellos Real, M., & Isoldi, L. A. (2020). Constructal Design for the ultimate buckling stress improvement of stiffened plates submitted to uniaxial compressive load. *Engineering Structures*, *203*, 109883. https://doi.org/10.1016/j.engstruct.2019.109883

Liu, H., Xi, K., Xie, Z., Lu, Z., Chen, H., Zhang, J., & Ge, Y. (2023). Constructal design of double-layer asymmetric flower baffles. *Energy*, *280*, 128254. https://doi.org/10.1016/j.energy.2023.128254

Lorente, S., Lee, J., & Bejan, A. (2010). The "flow of stresses" concept: the analogy between mechanical strength and heat convection. *International Journal of Heat and Mass Transfer*, *53*(15-16), 2963-2968. https://doi.org/10.1016/j.ijheatmasstransfer.2010.03.038

Lu, Z., Xie, Z., Xi, K., Lin, D., Liu, H., Ge, Y., & Wu, F. (2024). Constructal evolutionary design of liquid cooling heat sink embedded in 3D-IC based on deep neural network prediction. *International Communications in Heat and Mass Transfer*, *152*, 107273. https://doi.org/10.1016/j.icheatmasstransfer.2024.107273

Malikan, M., & Nguyen, V. B. (2018). A novel one-variable first-order shear deformation theory for biaxial buckling of a size-dependent plate based on Eringen's nonlocal differential law. *World Journal of Engineering*, *15*(5), 633-645. https://doi.org/10.1108/WJE-11-2017-0357

Milazzo, A., Benedetti, I., & Gulizzi, V. (2018). An extended Ritz formulation for buckling and post-buckling analysis of cracked multilayered plates. *Composite Structures*, *201*, 980-994. https://doi.org/10.1016/j.compstruct.2018.06.026

Milošević, M., Miltenović, A., Banić, M., & Tomić, M. (2017). Determination of residual stress in the rail wheel during quenching process by FEM simulation. *Facta Universitatis, Series: Mechanical Engineering*, *15*(3), 413-425. https://doi.org/10.22190/FUME170206029M

Mishurenko, N., & Semenov, A. (2024). Influence of Discretely Introduced Cutouts on the Buckling of Shallow Shells with Double Curvature. *Journal of Applied and Computational Mechanics*, *10*(1), 55-63. https://doi.org/10.22055/jacm.2023.44219.4182

Mitsui, K., Ikarashi, K., & Sada, K. (2024). Elastic Critical Buckling Coefficients for Skew Plates of Steel Structures under Biaxial Normal Stress. *Buildings*, *14*(4), 901. https://doi.org/10.3390/buildings14040901

Mohammadzadeh, B., Choi, E., & Kim, W. J. (2018). Comprehensive investigation of buckling behavior of plates considering effects of holes. *Struct. Eng. Mech*, *68*(2), 261-275. https://doi.org/10.12989/sem.2018.68.2.261

Moita, J. S., Araújo, A. L., Correia, V. F., Soares, C. M. M., & Herskovits, J. (2018). Material distribution and sizing optimization of functionally graded plate-shell structures. *Composites Part B: Engineering*, *142*, 263-272. https://doi.org/10.1016/j.compositesb.2018.01.023

Musmar, M. A. (2021). A Parametric Study on the Buckling Behavior of Square Steel Plates under Uniaxial Compression. https://doi.org/10.13189/cea.2021.090717

Narayanan, R., & Chow, F.-Y. (1984). Strength of biaxially compressed perforated plates. https://scholarsmine.mst.edu/cgi/viewcontent.cgi?article=1168&context=isccss

Nunes, B. R., Rodrigues, M. K., Oliveira Rocha, L. A., Labat, M., Lorente, S., dos Santos, E. D., Isoldi, L. A., & Biserni, C. (2021). Numerical-analytical study of earth-air heat exchangers with complex geometries guided by constructal design. *International Journal of Energy Research*, *45*(15), 20970-20987. https://doi.org/10.1002/er.7157

Park, J.-S., & Yi, M.-S. (2024). Root Causes of Thin-Plate Buckling Damage at the Aft-End in Crude Oil Tanker and Verification through Buckling Analysis. *Metals*, *14*(2), 158. https://doi.org/10.3390/met14020158

Pavlovic, A., & Fragassa, C. (2020). Geometry optimization by fem simulation of the automatic changing gear. *Reports in Mechanical Engineering*, *1*(1), 199-205. https://doi.org/10.31181/rme200101199p

Pavlovic, A., Fragassa, C., & Minak, G. (2017). Analiza izvijanja teleskopske dizalice: teorijska i numerička procjena kliznih oslonaca. *Tehnički vjesnik*, *24*(3), 729-735. https://doi.org/10.17559/TV-20160510143822

Piscopo, V. (2010). Refined buckling analysis of rectangular plates under uniaxial and biaxial compression. *International Journal of Mechanical and Mechatronics Engineering*, *4*(10), 1018-1025. https://doi.org/10.5281/zenodo.1078458

Qablan, H. A., Rabab'ah, S., Alfoul, B. A., & Hattamleh, O. A. (2022). Semi-empirical buckling analysis of perforated composite panel. *Mechanics Based Design of Structures and Machines*, *50*(8), 2635-2652. https://doi.org/10.1080/15397734.2020.1784198

Razera, A., da Fonseca, R., Isoldi, L., Dos Santos, E., Rocha, L., & Biserni, C. (2022). A constructal approach applied to the cooling of semi-elliptical blocks assembled into a rectangular channel under forced convection. *International Journal of Heat and Mass Transfer*, *184*, 122293. https://doi.org/10.1016/j.ijheatmasstransfer.2021.122293

Rocha, L., Santos, E. d., Cunha, D., Garcia, F., Lorenzini, G., Biserni, C., Letzow, M., Costa, J., Souza, J., & Isoldi, L. (2013). Constructal Design of Thermal Systems. *Constructal Law and the Unifying Principle of Design*, 295-321. https://doi.org/10.1007/978-1-4614-5049-8

Rocha, L. A., Lorente, S., & Bejan, A. (2018). Constructal theory in heat transfer. In *Handbook of thermal science and engineering* (pp. 329-360). Springer, Cham. https://doi.org/10.1007/978-3-319-32003-8_66-1

Saad-Eldeen, S., & Garbatov, Y. (2023). Experimental and Numerical Analysis of Structural Capacity of Perforated Stiffened Plates. *Journal of Marine Science and Engineering*, *11*(4), 842. https://doi.org/10.3390/jmse11040842

Saad-Eldeen, S., Garbatov, Y., & Soares, C. G. (2018). Structural capacity of plates and stiffened panels of different materials with opening. *Ocean Engineering*, *167*, 45-54. https://doi.org/10.1016/j.oceaneng.2018.08.013

Safaei, B., Onyibo, E. C., Goren, M., Kotrasova, K., Yang, Z., Arman, S., & Asmael, M. (2023). Free vibration investigation on RVE of proposed honeycomb sandwich beam and material selection optimization. *Facta Universitatis, Series: Mechanical Engineering*, *21*(1), 031-050. https://doi.org/10.22190/FUME220806042S

Shahani, A. R., & Kiarasi, F. (2023). Numerical and Experimental Investigation on Post-buckling Behavior of Stiffened Cylindrical Shells with Cutout subject to Uniform Axial Compression. *Journal of Applied and Computational Mechanics*, *9*(1), 25-44. https://doi.org/10.22055/jacm.2021.33649.2261

Shanmugam, N., & Narayanan, R. (1998). Ultimate Strength of Biaxially Loaded Plates. In *Stability and Ductility of Steel Structures (SDSS'97)* (pp. 211-223). Elsevier. https://doi.org/10.1016/B978-008043320-2/50020-4

Shanmugam, N., Thevendran, V., & Tan, Y. (1999). Design formula for axially compressed perforated plates. *Thin-Walled Structures*, *34*(1), 1-20. https://doi.org/10.1016/S0263-8231(98)00052-4

Shojaee, T., Mohammadi, B., Madoliat, R., & Salimi-Majd, D. (2019). Development of a finite strip method for efficient prediction of buckling and post-buckling in composite laminates containing a cutout with/without stiffener. *Composite Structures*, *210*, 538-552. https://doi.org/10.1016/j.compstruct.2018.11.007

Silveira, T., Pinto, V. T., Neufeld, J. P. S., Pavlovic, A., Rocha, L. A. O., Santos, E., & Isoldi, L. A. (2021). Applicability evidence of constructal design in structural engineering: Case study of biaxial elasto-plastic buckling of square steel plates with elliptical cutout. *Journal of Applied and Computational Mechanics*, *7*(2), 922-934. https://doi.org/10.22055/jacm.2021.35385.2647

Skripnyak, V. A., Iokhim, K., Skripnyak, E., & Skripnyak, V. V. (2021). Modeling of titanium alloys plastic flow in linear friction welding. *Facta Universitatis, Series: Mechanical Engineering*, *19*(1), 091-104. https://doi.org/10.22190/FUME201225014S

Szilard, R. (2004). Theories and applications of plate analysis: classical, numerical and engineering methods. *Appl. Mech. Rev.*, *57*(6), B32-B33. https://doi.org/https://books.google.com.pk/books/about/Theories_and_Applications_of_Plate_Analy.html?id=Hd3k

QURHXcoC&redir_esc=y

Trahair, N. S., Bradford, M., Nethercot, D., & Gardner, L. (2017). *The behaviour and design of steel structures to EC3*. CRC Press. https://doi.org/10.1201/9781315273518

Uslu, F., Saraçoğlu, M. H., & Albayrak, U. (2022). Buckling of square and circular perforated square plates under uniaxial loading. *Journal of Innovations in Civil Engineering and Technology*, *4*(2), 61-75. https://dergipark.org.tr/en/pub/jiciviltech/issue/74932/1190956

Wang, M., Chen, Y., Gao, W., Li, Z., & Zhang, J. (2024). Theoretical and numerical study of the buckling of steel-composite cylindrical shells under axial compression. *Applied Ocean Research*, *153*, 104221. https://doi.org/10.1016/j.apor.2024.104221

Yuan, T., Yang, Y., Kong, X., & Wu, W. (2021). Similarity criteria for the buckling process of stiffened plates subjected to compressive load. *Thin-Walled Structures*, *158*, 107183. https://doi.org/10.1016/j.tws.2020.107183

Zhang, Q., & Sun, Y. (2023). Statics, vibration, and buckling of sandwich plates with metamaterial cores characterized by negative thermal expansion and negative Poisson's ratio. *Applied Mathematics and Mechanics*, *44*(9), 1457-1486. https://doi.org/10.1007/s10483-023-3024-6

Zhang, Z., Feng, H., Chen, L., & Ge, Y. (2021). Multi-objective constructal design for compound heat dissipation channels in a three-dimensional trapezoidal heat generation body. *International Communications in Heat and Mass Transfer*, *127*, 105584. https://doi.org/10.1016/j.icheatmasstransfer.2021.105584

Zhang, Z., Ye, J., Huang, Z., Qin, G., & Xu, S. (2022). Elastic buckling behavior of corroded uniformly compressed plates with three simply supported edges. Structures,

Zureick, A.-H. (2018). On the buckling of an isotropic rectangular plate uniformly compressed on two simply supported edges and with two free unloaded edges. *Thin-Walled Structures*, *124*, 180-183. https://doi.org/10.1016/j.tws.2017.12.012

Appendix A

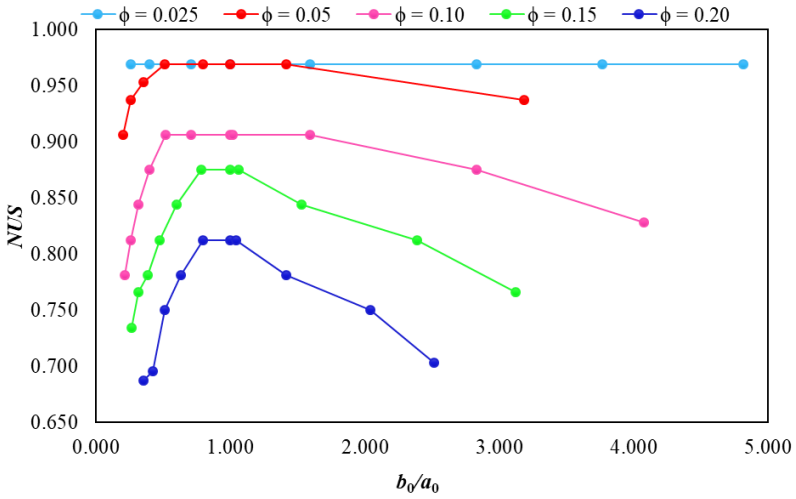

Figure A.1. Curves of the *NUS* for the Plates with $b/a = 1$ and $\alpha = 15°$.

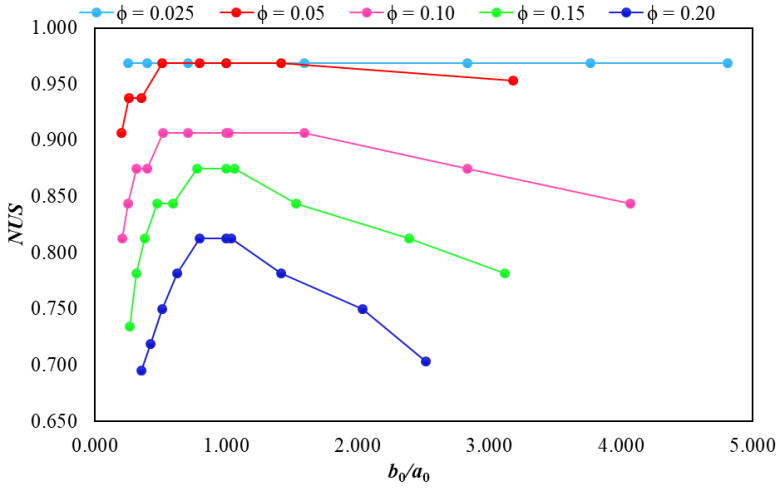

Figure A.2. Curves of the *NUS* for the Plates with $b/a = 1$ and $\alpha = 30°$.

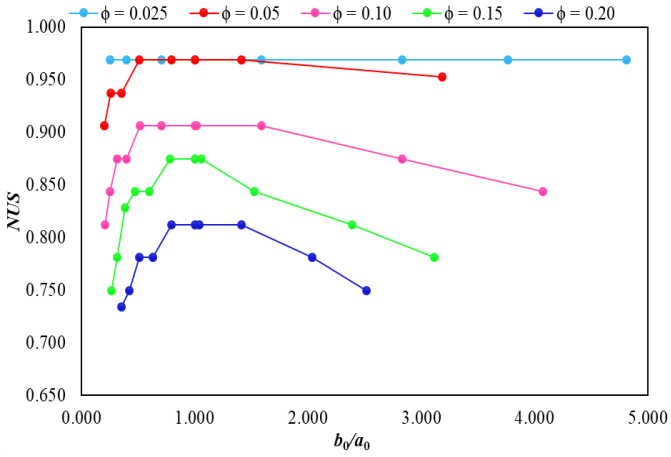

Figure A.3. Curves of the *NUS* for the Plates with $b/a = 1$ and $\alpha = 45°$.

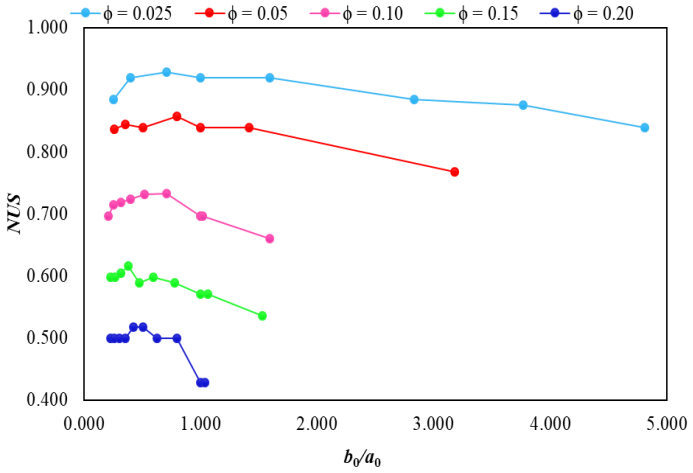

Figure A.4. Curves of the *NUS* for the Plates with $b/a = 0.5$ and $\alpha = 15°$.

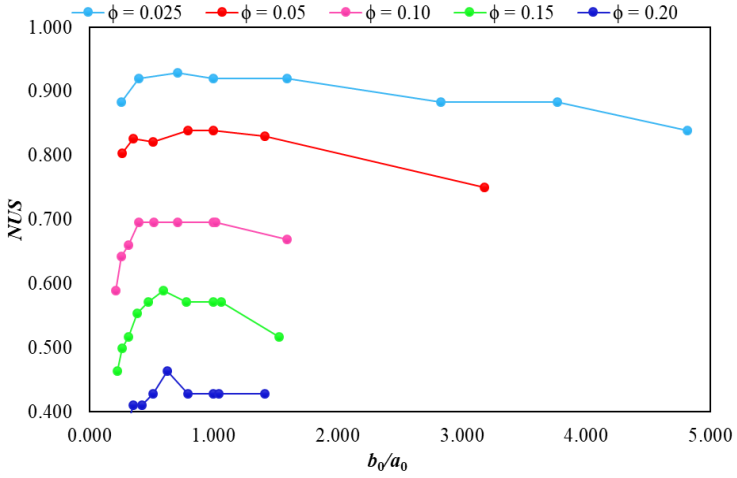

Figure A.5. Curves of the *NUS* for the Plates with $b/a = 0.5$ and $\alpha = 30°$.

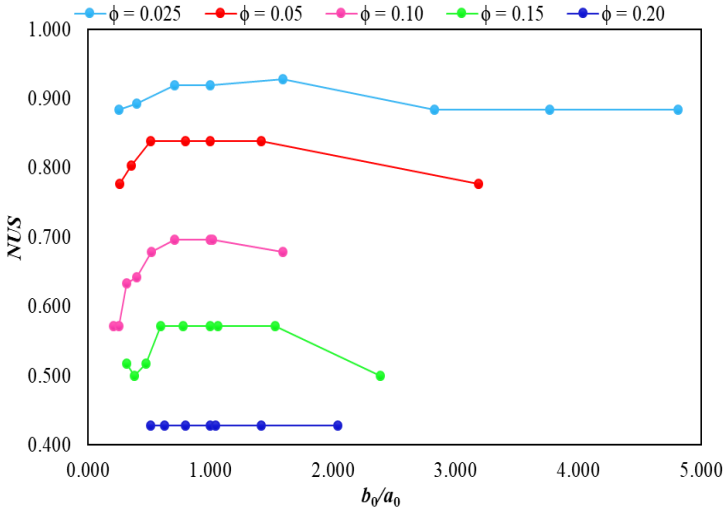

Figure A.6. Curves of the *NUS* for the Plates with $b/a = 0.5$ and $\alpha = 45°$.

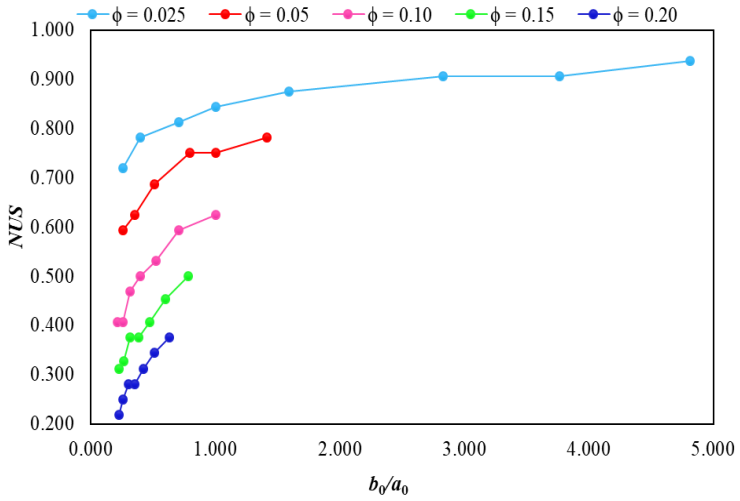

Figure A.7. Curves of the *NUS* for the Plates with $b/a = 0.25$ and $\alpha = 15°$.

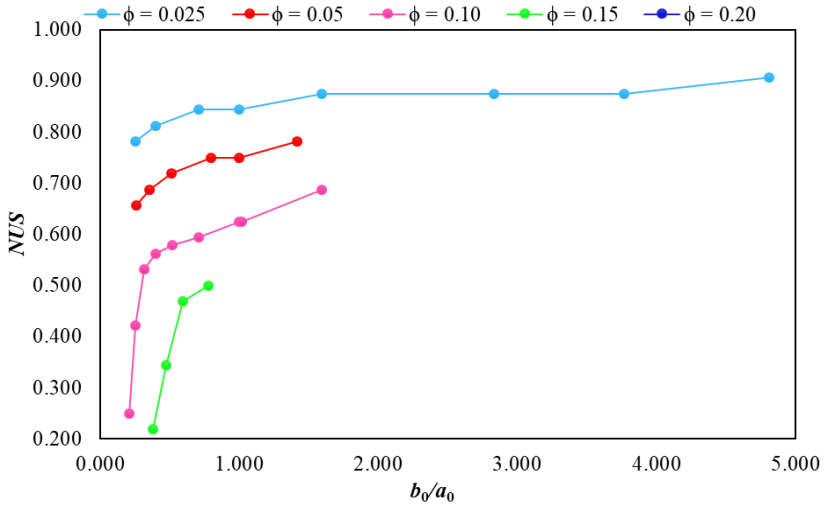

Figure A.8. Curves of the *NUS* for the Plates with $b/a = 0.25$ and $\alpha = 30°$.

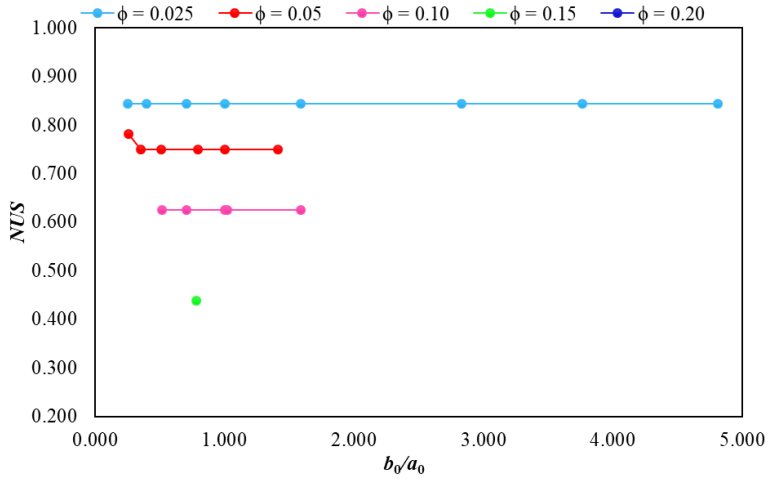

Figure A.9. Curves of the *NUS* for the Plates with $b/a = 0.25$ and $\alpha = 45°$.

Appendix B

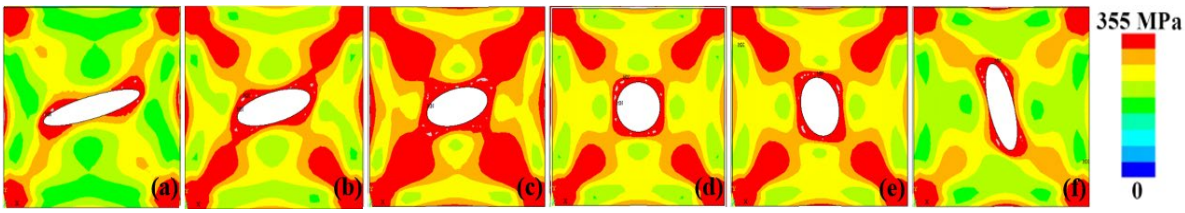

Figure B.1. Distribution of Von Mises Stresses for the Plates with $b/a = 1$, $\phi = 0.05$, and $\alpha = 15°$, being: (a) $b_0/a_0 = 0.199$; (b) $b_0/a_0 = 0.354$; (c) $b_0/a_0 = 0.509$; (d) $(b_0/a_0)_{2o} = 1.000$; (e) $b_0/a_0 = 1.415$; and (f) $b_0/a_0 = 3.183$.

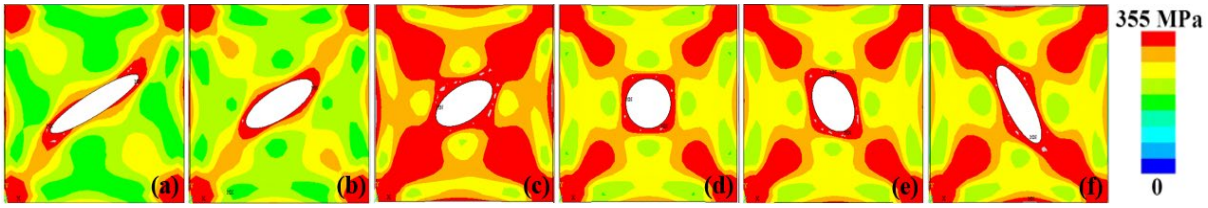

Figure B.2. Distribution of Von Mises Stresses for the Plates with $b/a = 1$, $\phi = 0.05$, and $\alpha = 30°$, being: (a) $b_0/a_0 = 0.199$; (b) $b_0/a_0 = 0.354$; (c) $b_0/a_0 = 0.509$; (d) $(b_0/a_0)_{2o} = 1.000$; (e) $b_0/a_0 = 1.415$; and (f) $b_0/a_0 = 3.183$.

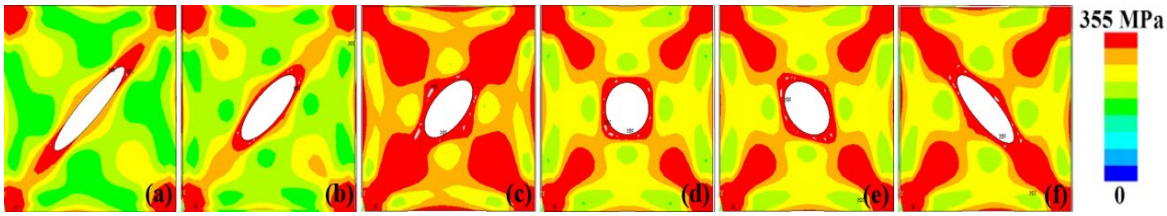

Figure B.3. Distribution of Von Mises Stresses for the Plates with $b/a = 1$, $\phi = 0.05$, and $\alpha = 45°$, being: (a) $b_0/a_0 = 0.199$; (b) $b_0/a_0 = 0.354$; (c) $b_0/a_0 = 0.509$; (d) $(b_0/a_0)_{2o} = 1.000$; (e) $b_0/a_0 = 1.415$; and (f) $b_0/a_0 = 3.183$.

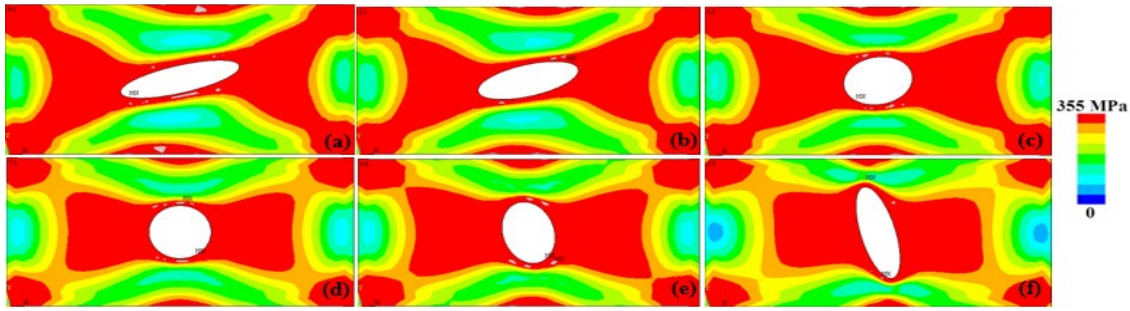

Figure B.4. Distribution of Von Mises Stresses for the Plates with $b/a = 0.5$, $\phi = 0.05$, and $\alpha = 15°$, being: (a) $b_0/a_0 = 0.260$; (b) $b_0/a_0 = 0.354$; (c) $(b_0/a_0)_o = 0.796$; (d) $b_0/a_0 = 1.000$; (e) $b_0/a_0 = 1.415$; and (f) $b_0/a_0 = 3.183$.

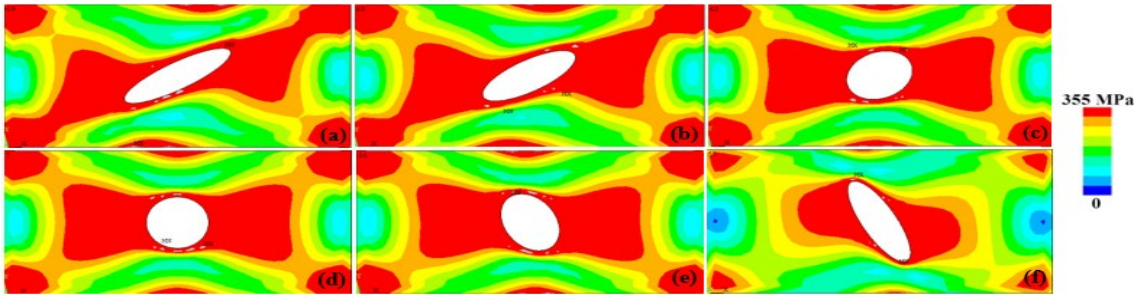

Figure B.5. Distribution of Von Mises Stresses for the Plates with $b/a = 0.5$, $\phi = 0.05$; and $\alpha = 30°$, being: (a) $b_0/a_0 = 0.260$; (b) $b_0/a_0 = 0.354$; (c) $(b_0/a_0)_o = 0.509$; (d) $b_0/a_0 = 1.000$; (e) $b_0/a_0 = 1.415$; and (f) $b_0/a_0 = 3.183$.

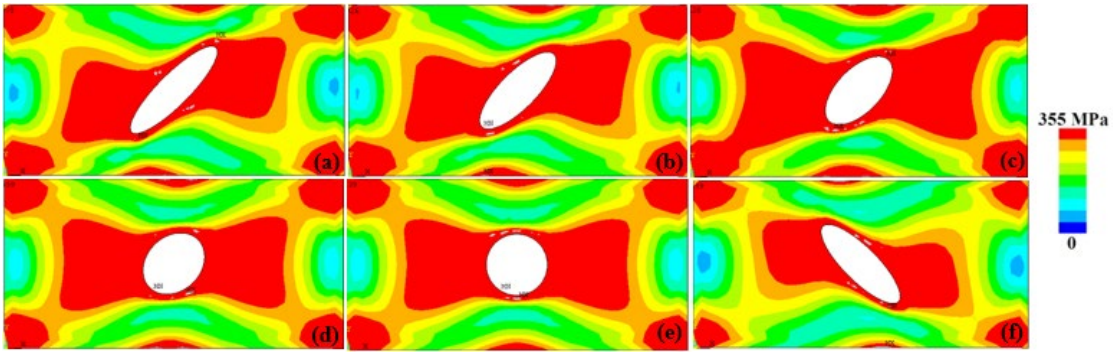

Figure B.6. Distribution of Von Mises Stresses for the Plates with $b/a = 0.5$, $\phi = 0.05$, and $\alpha = 45°$, being: (a) $b_0/a_0 = 0.260$; (b) $b_0/a_0 = 0.354$; (c) $(b_0/a_0)_o = 0.509$; (d) $b_0/a_0 = 1.000$; (e) $b_0/a_0 = 1.415$; and (f) $b_0/a_0 = 3.183$.

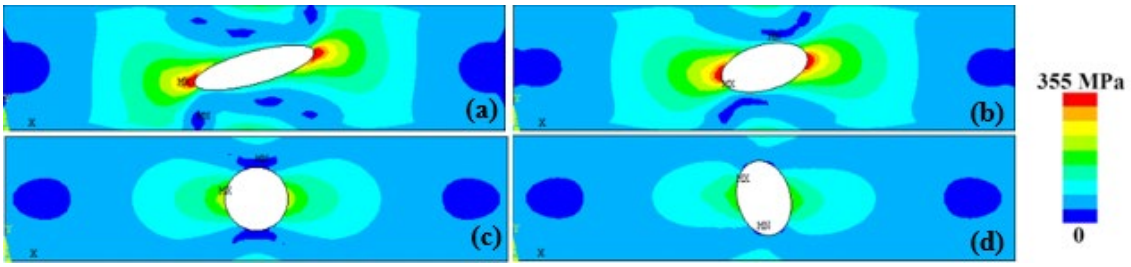

Figure B.7. Distribution of Von Mises Stresses for the Plates with $b/a = 0.25$, $\phi = 0.05$, and $\alpha = 15°$, being: (a) $b_0/a_0 = 0.260$; (b) $b_0/a_0 = 0.509$; (c) $b_0/a_0 = 1.000$; and (d) $(b_0/a_0)_o = 1.415$.

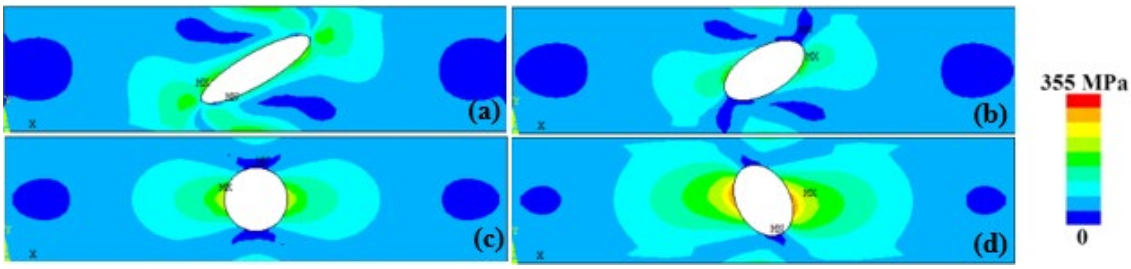

Figure B.8. Distribution of von Mises stresses for the plates with $b/a = 0.25$, $\phi = 0.05$, and $\alpha = 30°$, being: (a) $b_0/a_0 = 0.260$; (b) $b_0/a_0 = 0.509$; (c) $b_0/a_0 = 1.000$; and (d) $(b_0/a_0)_o = 1.415$.

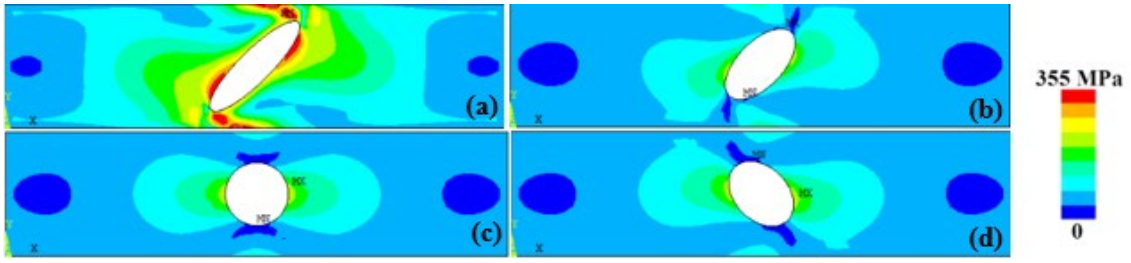

Figure B.9. Distribution of von Mises stresses for the plates with $b/a = 0.25$, $\phi = 0.05$, and $\alpha = 45°$, being: (a) $(b_0/a_0)_o = 0.260$; (b) $b_0/a_0 = 0.509$; (c) $b_0/a_0 = 1.000$; and (d) 1.415.

Glossary

Aspect Ratio: The proportion between the plate's length and width, affecting its buckling modes.
Boundary Conditions: Constraints applied to the edges of the plate that influence buckling behavior.
Buckling Load Factor: A multiplier indicating how close the applied load is to the calculated critical buckling load.
Circular/Elliptical Perforations: Openings in plates to optimize structural efficiency, affecting the buckling modes.
Constructal Design Method: A geometric evaluation method inspired by nature, aiming to improve the flow and

distribution of structures to minimize resistance or maximize efficiency.

Critical Load: The minimum load at which buckling occurs.

Elastic Buckling: Deformation of a structure under critical load, with the material remaining in the elastic range.

Elasto-plastic Buckling: Buckling involving both elastic and plastic deformation, occurring after the yield point.

Exhaustive Search Technique: An optimization technique where all possible configurations are explored to find the best design.

Finite Element Method (FEM): A numerical simulation technique used to study buckling behavior by dividing the structure into smaller, solvable elements.

Imperfections: Small geometric irregularities in plates that can affect buckling behavior.

Linear vs. Nonlinear Analysis: Linear assumes small deformations, while nonlinear includes large displacements and plasticity effects.

Load Factor: The ratio of the applied load to the critical load, used to predict structural stability.

Load-bearing Capacity: The maximum load a plate can sustain before buckling failure.

Material Anisotropy: The property of materials having different mechanical characteristics in different directions, relevant in buckling analysis.

Mode Shapes: The various deformation patterns a plate can exhibit when buckling.

Optimization: The process of adjusting geometric parameters (e.g., perforation size, perforation shape, perforation type) to improve resistance to buckling.

Perforated Plates: Steel plates with circular or elliptical holes to reduce weight or optimize material distribution.

Plastic Hinge Formation: Localized plastic deformation in a plate affecting its post-buckling behavior.

Post-Buckling Behavior: Analysis of how the structure behaves after initial buckling, especially in elasto-plastic scenarios.

Residual Stresses: Stresses present in the material before external loads, influencing buckling behavior.

Safety Factor: A design margin used to prevent buckling failure, especially for elasto-plastic materials.

Slenderness Ratio: The ratio of a plate's height to its thickness, determining susceptibility to buckling.

Stiffness Matrix: A matrix in FEM representing a structure's resistance to deformation under load.

Stress Concentration: Increased stress around perforations or holes, influencing the plate's resistance to buckling.

Structural Integrity: Evaluation of a perforated plate's ability to maintain functionality without buckling.

Thickness Ratio: The ratio of plate thickness to other dimensions, which affects its buckling resistance.

Ultimate Buckling Load: The maximum load that a structural component can sustain before it experiences buckling failure.

von Mises Stress: A criterion for predicting when a material will start to deform plastically.

Yield Point: The point at which material transitions from elastic to plastic deformation.